Lagrangian structures and the rate of strain in a partition of two-dimensional turbulence

G. Haller
Division of Applied Mathematics, Lefschetz Center for Dynamical Systems, Brown University, Providence, Rhode Island 02912

(Received 22 February 2001; accepted 20 June 2001)

We derive analytic criteria for the existence of hyperbolic (attracting or repelling), elliptic, and parabolic material lines in two-dimensional turbulence. The criteria use a frame-independent Eulerian partition of the physical space that is based on the sign definiteness of the strain acceleration tensor over directions of zero strain. For Navier–Stokes flows, our hyperbolicity criterion can be reformulated in terms of strain, vorticity, pressure, viscous and body forces. The special material lines we identify allow us to locate different kinds of material structures that enhance or suppress finite-time turbulent mixing: stretching and folding lines, Lagrangian vortex cores, and shear jets. We illustrate the use of our criteria on simulations of two-dimensional barotropic turbulence. © *2001 American Institute of Physics.* [DOI: 10.1063/1.1403336]

I. INTRODUCTION

A goal in this paper is to provide mathematically exact and frame-independent criteria for the identification of *Lagrangian coherent structures* in two-dimensional turbulence. Roughly speaking, such structures are special material lines that have a major influence on the kinematics of mixing over finite time intervals. We aim to classify these structures and provide computable criteria that can be used to locate them in numerical or experimental velocity data.

Lagrangian coherent structures have long been recognized in models of two-dimensional chaotic advection: stable and unstable manifolds and KAM tori are all material lines that either enhance or inhibit mixing (see, e.g., Aref and El Naschie[1] for a recent review and Rom-Kedar[2] for further developments). These structures have first been studied in the nonlinear dynamical systems literature and then adopted to explain features of fluid flows with periodic or quasiperiodic, i.e., regular time dependence. It turns out, however, that assuming exact periodicity for a flow field is a more far-reaching assumption than one might first think. Being able to generate the flow for *all times* from a one-period velocity sample is crucial in order to define classical stable and unstable manifolds. In this sense chaotic advection, with its attendant homoclinic tangles and lobes, has a solid foundation only for regularly repeating velocity fields defined over infinite time intervals. While such velocity fields are relevant in a number of applications and first-order models, turbulent flows admit general time dependence, a fact that prevents the extrapolation from a finite-time velocity sample to infinite times. As a result, all traditional definitions of stability, instability, or neutral behavior are naturally lost. The problem, however, is not just a matter of definitions: complicated geometric structures such as chaotic tangles or KAM tori that are typical in infinite-time periodic or quasiperiodic velocity fields (cf. Ottino[3]) simply do not exist in finite-time turbulent data sets, as they are ''artifacts'' of the periodic or quasiperiodic assumption on the underlying velocity field. One can still seek such structures in special infinite-time, nonperiodic flows with certain uniformly recurrent features (see Malhotra and Wiggins[4]). However, it appears that understanding the Lagrangian dynamics of real-life nonperiodic flow data requires new approaches.

Two-dimensional turbulent flows clearly admit Lagrangian organizing structures, as evidenced by the existence of vortex cores and material filaments in detailed numerical simulations (see, e.g., Elhmaïdi *et al.*[5] and Ziemniak *et al.*[6]). As a first attempt, one may try to infer the location of these Lagrangian coherent structures from instantaneous streamline configurations. In particular, one may release trial material lines near ''Eulerian'' unstable manifolds found in instantaneous plots of the velocity field, and expect that they converge to actual Lagrangian coherent structures. This technique was apparently first employed in Ridderinkhof and Loder[7] for a numerically generated periodic velocity field, followed by several works on more general velocity fields (see Miller *et al.*,[8] Rogerson *et al.*,[9] Koh and Plumb,[10] and Coulliette and Wiggins[11]). Studying this approach, Haller and Poje[12] gave a mathematical criterion under which Eulerian unstable manifolds indeed indicate a multitude of nearby *finite-time unstable manifolds* for the Lagrangian dynamics (see Poje and Haller[13] and Velasco Fuentes[14] for applications of the criterion). They also showed how violating the criterion may lead to ''phoney'' Lagrangian structures. To avoid the frame-dependent nature of the stagnation point-based approach, Bowman[15] has suggested relative dispersion (''finite strain'') as a diagnostic tool to find finite-time unstable manifolds in atmospheric flows with no stagnation points (see also Jones and Winkler[16] and Winkler[17]). This approach is essentially a quick and smooth way of approximating finite-time Lyapunov exponent plots that tend to reveal similar structures (see, e.g., Pierrehumbert[18] and Pierrehumbert and

Yang[19]). As a further step in this direction, Joseph and Legras[20] have recently employed finite-size Lyapunov exponents in the detection of finite-time invariant manifolds in atmospheric flows. The connection between Lagrangian average velocities (Malhotra *et al.*[21] and Mezić and Wiggins[22]) and finite-time Lagrangian structures in turbulence was studied numerically in Poje *et al.*[23]

In an effort to locate Lagrangian coherent structures (LCS) rigorously without the use of stagnation points, Haller[24] proved a Lagrangian version of the Okubo–Weiss criterion (cf. Sec. V A) that identifies finite-time invariant manifolds in a Galilean-invariant way. Haller and Yuan[25] simplified this ''$\alpha-\beta$ criterion'' for incompressible flows and showed how Lagrangian coherent structures (LCS) can be defined and found rigorously in general turbulent flows. They identify attracting LCS (distinguished finite-time unstable manifolds) and repelling LCS (distinguished finite-time stable manifolds) in general velocity fields. This approach is Galilean-invariant, but still frame-dependent, i.e., gives different results in different rotating frames. Exploiting this frame dependence, Lapeyre *et al.*[26] suggested that for better results, the $\alpha-\beta$ criterion should be applied in a frame co-rotating with the eigenvectors of the rate of strain (cf. Sec. V B). A three-dimensional extension of the $\alpha-\beta$ criterion appears in Haller,[27] where attracting and repelling material surfaces and lines are located for time-dependent three-dimensional flows.

A shortcoming of the above analytic approaches to LCS is their dependence on the coordinate frame. This makes it difficult to locate regions of intense Lagrangian mixing in a variety of flows that admit a nonzero and spatially nonuniform mean velocity. Since such flows rarely display closed streamfunction contours and stagnation points, one does not quite know where to look for regions of distinguished Lagrangian behavior. Passing to an appropriate moving frame will generally introduce stagnation points and closed contours. However, one can create such structures in any designated flow region via appropriate time-dependent coordinate changes, a fact that questions the distinguished role of any Eulerian coherent structure created by a change of frame. Several important flows of geophysical fluid dynamics pose related challenges, including those with meandering jets such as the Gulf Stream, or wave breaking events such as those observed on the edge of the stratospheric polar vortex. All this calls for a new approach to LCS that is fully frame-independent, i.e., invariant under time-dependent rotations and translations.

Motivated by the above need, in this paper a new frame-independent way of locating Lagrangian coherent structures in two-dimensional turbulence is offered. Taking a Lyapunov function approach to the stability of individual fluid trajectories, we obtain a partition of the physical space into elliptic, parabolic, and hyperbolic regions (EPH) based on the definiteness of the strain acceleration tensor over directions of zero strain. When viewed instantaneously, these regions turn out to coincide with those that one would infer from the application of a nonrigorous Eulerian principle, the Okubo–Weiss criterion in the strain basis (cf. Sec. V B). However, we extend these regions in space-time over a time interval I, and prove properties of material lines that spend longer times in the corresponding elliptic, parabolic, and hyperbolic sets, $\mathcal{E}(I)$, $\mathcal{P}(I)$, and $\mathcal{H}(I)$. In particular, attracting or repelling material lines either stay in $\mathcal{H}(I)$ or stray into the elliptic regions for short times that we can estimate from above. Elliptic material lines stay in $\mathcal{E}(I)$ for longer times that we can estimate from below, and parabolic lines stay in $\mathcal{P}(I)$. This approach gives a fully frame-independent way of locating Lagrangian coherent structures (LCS), the locally most robust hyperbolic, elliptic, and parabolic material lines. Hyperbolic LCS are responsible for advective mixing over finite-time intervals: in particular, *stretch lines* split up fluid blobs that in turn are attracted to *fold lines*. We define elliptic LCS as Lagrangian *vortex cores* that inhibit mixing, and parabolic LCS as *shear jets*.

As an interesting side-result, we derive a version of our criteria that predicts Lagrangian finite-time hyperbolicity purely in terms of strain, vorticity, pressure, viscous, and body forces for incompressible Navier–Stokes flows (cf. Sec. IV C). This result offers hope that the approach we propose in this paper will ultimately lead to an understanding of physical causes behind increased mixing in specific regions of a turbulent flow.

We also propose and test different ways to visualize the above Lagrangian structures in finite-time velocity data. We apply these techniques to extract Lagrangian coherent structures from numerical simulations of barotropic turbulence (cf. Provenzale *et al.*[28]). We conclude the paper with a summary of our results and a list of open questions.

II. RATE OF STRAIN, ZERO STRAIN SET, AND STRAIN ACCELERATION

Consider a two-dimensional velocity field $\mathbf{v}(\mathbf{x},t)$ defined on some finite time interval $\mathcal{I}$. For simplicity, we shall assume that the flow generated by $\mathbf{v}$ is incompressible, i.e., $\nabla\cdot\mathbf{v}\equiv\mathbf{0}$. We shall use the notation

$$\mathbf{S}=\tfrac{1}{2}(\nabla\mathbf{v}+(\nabla\mathbf{v})^T),$$

for the rate-of-strain tensor. Note that by incompressibility, either $\det(\mathbf{S})\neq 0$ or $\mathbf{S}=\mathbf{0}$ holds for any $\mathbf{x}$ and t. We also recall that for an infinitesimal line element $\boldsymbol{\xi}(t)$ advected along a fluid particle, we have

$$\frac{1}{2}\frac{d}{dt}|\boldsymbol{\xi}|^2=\langle\boldsymbol{\xi},\mathbf{S}\boldsymbol{\xi}\rangle, \tag{1}$$

where $\langle\cdot,\cdot\rangle$ denotes the usual Euclidean inner product. By incompressibility, if $\mathbf{S}$ is nonsingular, then it admits a positive and a negative eigenvalue that add up to zero. In such a case the zero strain set,

$$Z=\{\boldsymbol{\xi}|\langle\boldsymbol{\xi},\mathbf{S}\boldsymbol{\xi}\rangle=0\}, \tag{2}$$

is a set of two orthogonal lines. In a general turbulent flow the diagonal elements of $\mathbf{S}$ are typically nonzero, in which case Z is spanned by the vectors

$$\boldsymbol{\xi}^-(\mathbf{x},t)=\begin{pmatrix} s_{22} \\ -s_{12}-|\mathbf{S}|/\sqrt{2}\end{pmatrix},\ \boldsymbol{\xi}^+(\mathbf{x},t)=\begin{pmatrix} s_{22} \\ -s_{12}+|\mathbf{S}|/\sqrt{2}\end{pmatrix}, \tag{3}$$

with s_{ij} denoting the entries of $\mathbf{S}$ and $|\mathbf{S}|=\sqrt{\Sigma_{i,j}s_{ij}^2}$ referring to the Euclidean matrix norm of $\mathbf{S}$.[29] Note that Z depends on $\mathbf{x}$ and t, but we suppress this for notational simplicity. The length of the vectors $\boldsymbol{\xi}^{\pm}$ will play no role in our analysis so they can be normalized to one. In the expressions above we omitted this normalization for simplicity.

A further important quantity will be the symmetric matrix[30]

$$\mathbf{M}=\dot{\mathbf{S}}+2\mathbf{S}\nabla\mathbf{v}, \tag{4}$$

where $\dot{\mathbf{S}}=\mathbf{v}\cdot\nabla\mathbf{S}+(\partial/\partial t)\,\mathbf{S}$ is the material derivative of $\mathbf{S}$.[31,32] We shall refer to $\mathbf{M}$ as the *strain acceleration* tensor, since for the line element $\boldsymbol{\xi}$ introduced above,

$$\frac{1}{2}\frac{d^2}{dt^2}|\boldsymbol{\xi}|^2=\langle\boldsymbol{\xi},\mathbf{M}\boldsymbol{\xi}\rangle. \tag{5a}$$

In continuum mechanical terms, $\mathbf{M}$ is a physically objective material derivative of $\mathbf{S}$, sometimes called the Cotter–Rivlin derivative of $\mathbf{S}$ (see Cotter and Rivlin[33] or Béda *et al.*[34]).

We shall denote the restriction of the tensor $\mathbf{M}$ to the zero strain set Z by $\mathbf{M}_Z$, i.e., we let

$$\mathbf{M}_Z=\mathbf{M}|_Z. \tag{5b}$$

We call $\mathbf{M}_Z$ *positive/negative definite, semidefinite, or indefinite* if $\langle\boldsymbol{\xi},\mathbf{M}\boldsymbol{\xi}\rangle$ is a positive/negative definite, semidefinite, or indefinite quadratic form for $\boldsymbol{\xi}\in Z$. Incompressibility turns out to imply the following property of $\mathbf{M}_Z$.

Proposition 1: *If* $\mathbf{S}$ *is nonvanishing, then* $\mathbf{M}_Z$ *is either positive definite, positive semidefinite, or indefinite.*

This proposition will follow from a result in Sec. III B (cf. the discussion after Proposition 2).

III. LOCAL FLOW GEOMETRY NEAR A FLUID TRAJECTORY

A. Linearized flow

Let $\mathbf{x}(t)$ be a trajectory generated by the velocity field $\mathbf{v}(\mathbf{x},t)$. The linearized velocity field along $\mathbf{x}(t)$ can be written as

$$\dot{\boldsymbol{\xi}}=\mathbf{A}(t)\boldsymbol{\xi}, \tag{6}$$

where $\mathbf{A}(t)=\nabla\mathbf{v}(\mathbf{x}(t),t)$, and $\boldsymbol{\xi}$ is a two-dimensional vector. If $\mathbf{S}\neq\mathbf{0}$ at some time t, then the zero strain set defined in (2) divides the phase plane of (6) into four quadrants, as shown in Fig. 1. Inside the regions formed by two facing quadrants, the quadratic form,

$$C(\boldsymbol{\xi},t)=\langle\boldsymbol{\xi},\mathbf{S}(\mathbf{x}(t),t)\boldsymbol{\xi}\rangle,$$

assumes negative values, whereas in the remaining two quadrants it takes positive values. By (1), this means that vectors in the former quadrants shrink instantaneously, while vectors in the latter two quadrants expand. Let $\mathcal{C}$ denote the unit circle of the $\boldsymbol{\xi}$-plane, and let $\Psi^-(t)$ and $\Psi^+(t)$ denote the two closed sectorial regions inside $\mathcal{C}$ that are bounded by the lines $\boldsymbol{\xi}^-$ and $\boldsymbol{\xi}^+$ (see Fig. 1). By the above discussion, at time t solutions of (6) penetrate into $\Psi^-(t)$ and leave $\Psi^+(t)$ along the perimeter of the unit circle.

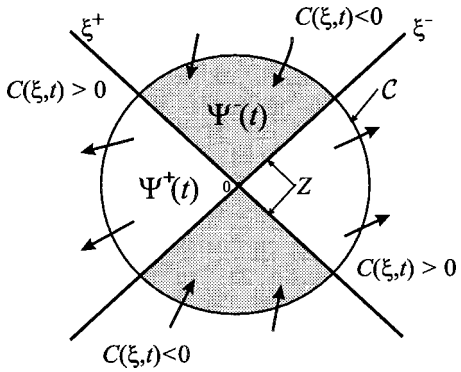

FIG. 1. The sectors $\Psi^+(t)$ and $\Psi^-(t)$ of the unit circle $\mathcal{C}$.

While the behavior of solutions relative to the circle $\mathcal{C}$ is clear both for zero and nonzero rate of strain, it is not immediately clear whether solutions lying instantaneously on the zero strain set Z cross from $\Psi^+(t)$ to $\Psi^-(t)$ or the other way around. However, a simple Lyapunov function-type argument can be used to decide which way the solutions cross: trajectories along the vector $\boldsymbol{\xi}^{\pm}$ are instantaneously crossing from the sector $\Psi^-(t)$ to $\Psi^+(t)$ if the function $C(\boldsymbol{\xi},t)$ is instantaneously increasing along Z, i.e.,

$$\frac{d}{dt}C(\boldsymbol{\xi}^{\pm}(t),t)=\langle\boldsymbol{\xi}^{\pm},\mathbf{M}\boldsymbol{\xi}^{\pm}\rangle>0, \tag{7}$$

or from $\Psi^+(t)$ to $\Psi^-(t)$ if

$$\frac{d}{dt}C(\boldsymbol{\xi}^{\pm}(t),t)=\langle\boldsymbol{\xi}^{\pm},\mathbf{M}\boldsymbol{\xi}^{\pm}\rangle<0. \tag{8}$$

Trajectories are instantaneously tangent to the boundaries of the above sectors whenever

$$\frac{d}{dt}C(\boldsymbol{\xi}^{\pm}(t),t)=\langle\boldsymbol{\xi}^{\pm},\mathbf{M}\boldsymbol{\xi}^{\pm}\rangle=0. \tag{9}$$

By incompressibility, the possible sign combinations of $\langle\boldsymbol{\xi}^+,\mathbf{M}\boldsymbol{\xi}^+\rangle$ and $\langle\boldsymbol{\xi}^-,\mathbf{M}\boldsymbol{\xi}^-\rangle$ are limited: only one of them can be nonpositive at a time, as we stated more formally in Proposition 1.

The observations made in this section imply that the local instantaneous flow geometry near the $\boldsymbol{\xi}=\mathbf{0}$ solution of (6) falls in one of the four categories shown in Fig. 2. Note that these pictures show the behavior of particles in a frame that is co-rotating with $\boldsymbol{\xi}^+(t)$ and $\boldsymbol{\xi}^-(t)$ (whenever these vectors are nonzero). The indexing of $\boldsymbol{\xi}^+(t)$ and $\boldsymbol{\xi}^-(t)$ has no significance and hence can be interchanged.

Despite the fact that we have information about the instantaneous velocity field geometry from Eqs. (7)–(9), one cannot immediately guess the actual stability type of the underlying trajectory $\mathbf{x}(t)$ in cases (a) and (c), since the exact solutions of (6) are not available. However, if the trajectory stays in regions where $\mathbf{S}=\mathbf{0}$ [Fig. 2(d)] or where $\mathbf{M}_Z$ is positive semidefinite [Fig. 2(b)] over a *period* of time, the exact linearized dynamics can be explicitly calculated.

In case (d), a direct integration of (6) yields the solution

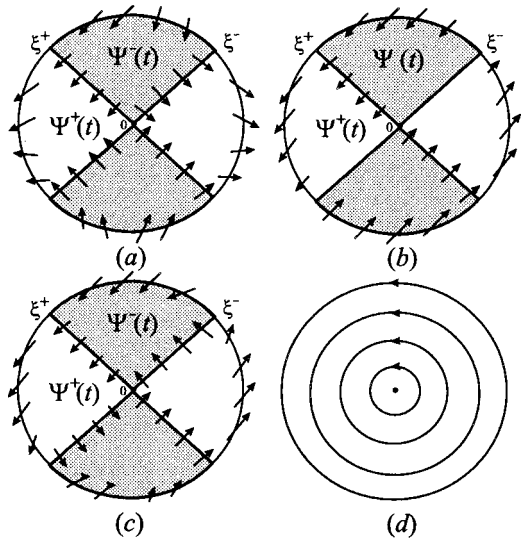

FIG. 2. Instantaneous linearized flow geometry near $\mathbf{x}(t)$ for the four basic cases: (a) Saddle-type flow, i.e., $\langle \boldsymbol{\xi}^+, \mathbf{M}\boldsymbol{\xi}^+ \rangle > 0$ and $\langle \boldsymbol{\xi}^-, \mathbf{M}\boldsymbol{\xi}^- \rangle > 0$. (b) Shear-type flow, i.e., $\langle \boldsymbol{\xi}^+, \mathbf{M}\boldsymbol{\xi}^+ \rangle > 0$ and $\langle \boldsymbol{\xi}^-, \mathbf{M}\boldsymbol{\xi}^- \rangle = 0$. (c) Elliptic rotation, i.e., $\langle \boldsymbol{\xi}^+, \mathbf{M}\boldsymbol{\xi}^+ \rangle > 0$ and $\langle \boldsymbol{\xi}^-, \mathbf{M}\boldsymbol{\xi}^- \rangle < 0$. (d) Pure rotation, i.e., $\mathbf{S} = \mathbf{0}$.

$$\boldsymbol{\xi}(t) = \begin{pmatrix} \cos \int_{t_0}^{t} \omega(\tau)\, d\tau & -\sin \int_{t_0}^{t} \omega(\tau)\, d\tau \\ \sin \int_{t_0}^{t} \omega(\tau)\, d\tau & \cos \int_{t_0}^{t} \omega(\tau)\, d\tau \end{pmatrix} \boldsymbol{\xi}_0,$$

where $\pm\omega(\tau)$ denote the off-diagonal elements of $\mathbf{A}(t)$. This reveals an elliptic stability type for (6) over any finite time interval. In case (b), one can pass to a frame co-rotating with the vectors $\boldsymbol{\xi}^+$ and $\boldsymbol{\xi}^-$. Denoting the new coordinates by (x^+, x^-), respectively, and using the facts that $\dot{x}^+|_{x^+=0} = 0$ and $\dot{x}^-|_{x^+>0} < 0$, we can rewrite (6) in the new basis as

$$\begin{pmatrix} \dot{x}^- \\ \dot{x}^+ \end{pmatrix} = \begin{pmatrix} 0 & -\nu^2(t) \\ 0 & 0 \end{pmatrix} \begin{pmatrix} x^- \\ x^+ \end{pmatrix},$$

which admits the solution

$$x^-(t) = x_0^- - x_0^+ \int_{t_0}^{t} \nu^2(\tau) d\tau,\ x^+(t) \equiv x_0^+ . \tag{10}$$

Therefore, in the original basis one obtains a parallel shear flow co-rotating with the set of zero strain Z.

B. Local flux

Back to the full nonlinear velocity field $\mathbf{v}(\mathbf{x},t)$, we want to introduce a quantity that characterizes the rate of local stirring near the trajectory $\mathbf{x}(t)$. Assume that the trajectory is at the point $\mathbf{x}_0$ at time t. We first define $\mathcal{S}_\epsilon(\mathbf{x}_0)$ as the circle of radius ϵ centered at the point $\mathbf{x}_0$, then define the *local flux* at $\mathbf{x}_0$ as

$$\varphi(\mathbf{x}_0,t) = \lim_{\epsilon \to 0} \frac{1}{2\epsilon^2} \int_{\mathcal{S}_\epsilon(\mathbf{x}_0)} |(\mathbf{v}(\mathbf{x},t) - \mathbf{v}(\mathbf{x}_0,t)) \cdot \mathbf{n}|\, ds, \tag{11}$$

where $\mathbf{n}$ denotes the inward unit normal at any point of $\mathcal{S}_\epsilon(\mathbf{x}_0)$. Note that $\varphi(\mathbf{x}_0,t) \geqslant 0$ by definition.

To interpret the above definition, we first note that $\mathbf{v}(\mathbf{x},t) - \mathbf{v}(\mathbf{x}_0,t)$ is the relative velocity of the fluid particle at $\mathbf{x}$ in the frame co-moving with $\mathbf{x}(t)$, the trajectory currently at $\mathbf{x}_0$. Thus, without the ϵ^2 normalizing factor, the integral in (11) gives the relative flux into the ball bounded by $\mathcal{S}_\epsilon(\mathbf{x}_0)$. This quantity is then normalized by ϵ^2, a factor proportional to the area of the ϵ-circle. Accordingly, the dimension of $(\mathbf{x}_0,t)$ is $[1/s]$. Since φ is defined at any point of the physical space, from now on we shall omit the 0 subscript from its spatial argument.

It turns out that the local flux is directly related to the eigenvalues of $\mathbf{S}(\mathbf{x},t)$. Moreover, it can be written as the sum of two frame-independent quantities that will be very useful later.

Proposition 2:

(i) *We have*

$$\varphi(\mathbf{x},t) = \sqrt{2}\,|\mathbf{S}(\mathbf{x},t)|.$$

(ii) *Assume that* $\mathbf{S}(\mathbf{x},t) \neq \mathbf{0}$. *Then*

$$\varphi(\mathbf{x},t) = \varphi^+(\mathbf{x},t) + \varphi^-(\mathbf{x},t),$$

where

$$\varphi^\pm = \frac{1}{2} \frac{\langle \boldsymbol{\xi}^\pm, \mathbf{M}\boldsymbol{\xi}^\pm \rangle}{|\boldsymbol{\xi}^\pm||\mathbf{S}\boldsymbol{\xi}^\pm|}. \tag{12}$$

This proposition is proved in Sec. 1 of the Appendix. Note that by statement (i) the local flux is simply a scalar multiple of the norm of the rate-of-strain tensor.

From the proof of Proposition 2 one can see the physical meaning of $\varphi^\pm$: they give the (normalized) instantaneous net flux through the appropriate component $\boldsymbol{\xi}^\pm$ of the zero strain set. They are positive for fluxes from the sector $\Psi^-(t)$ into $\Psi^+(t)$. Statement (ii) implies that either φ^+ or φ^- must be non-negative since φ is non-negative by definition. Thus either $\langle \boldsymbol{\xi}^+, \mathbf{M}\boldsymbol{\xi}^+ \rangle$ or $\langle \boldsymbol{\xi}^-, \mathbf{M}\boldsymbol{\xi}^- \rangle$ must be non-negative, which proves Proposition 1. As we shall see later, the fluxes $\varphi^\pm$ will have a fundamental role in identifying the exact stability type of the linearized velocity field (6).

IV. A MIXING-BASED PARTITION OF TWO-DIMENSIONAL TURBULENCE

We consider the velocity field $\mathbf{v}(\mathbf{x},t)$ and seek to construct a partition of the physical space at a given time t into regions that exhibit qualitatively different Lagrangian mixing properties. Based on our discussion in Sec. III A (cf. Fig. 2) and Proposition 2, at any time t we can uniquely partition the physical space into the following three regions.

The *elliptic region* $\mathcal{E}(t)$: the set of points where $\mathbf{M}_Z(\mathbf{x},t)$ is indefinite *or* $\mathbf{S}(\mathbf{x},t)$ vanishes.

The *parabolic region* $\mathcal{P}(t)$: the set of points where $\mathbf{M}_Z(\mathbf{x},t)$ is positive semidefinite.

The *hyperbolic region* $\mathcal{H}(t)$: the set of points where $\mathbf{M}_Z(\mathbf{x},t)$ is positive definite.

For a fixed time interval I, we then define the elliptic, parabolic, and hyperbolic sets $\mathcal{E}(I)$, $\mathcal{P}(I)$, and $\mathcal{H}(I)$ as domains in space–time that are spanned by the above time-dependent regions over the time interval I:

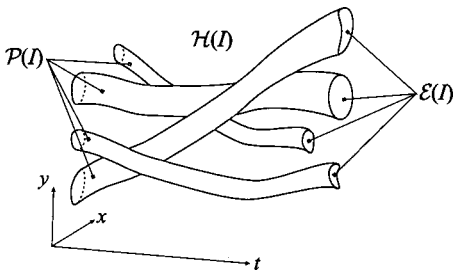

FIG. 3. A sketch of the elliptic, parabolic, and hyperbolic sets in space–time.

$$\mathcal{E}(I)=\{(\mathbf{x},t)|\mathbf{x}\in\mathcal{E}(t),t\in I\},$$

$$\mathcal{P}(I)=\{(\mathbf{x},t)|\mathbf{x}\in\mathcal{P}(t),t\in I\},$$

$$\mathcal{H}(I)=\{(\mathbf{x},t)|\mathbf{x}\in\mathcal{H}(t),t\in I\}.$$

In a general two-dimensional flow the elliptic set is typically a union of tubes, the parabolic set is the union of the cylinders bounding these tubes, and the hyperbolic set is the region outside the tubes (see Fig. 3).

For brevity, we shall refer to the above partition of the physical space as the *EPH partition*, with the acronym standing for Elliptic–Parabolic–Hyperbolic. As opposed to instantaneous Eulerian partitions of turbulent flows that have been suggested previously (cf. Sec. V), the quantities used in the EPH partition will allow us to deduce Lagrangian features of fluid trajectories in a mathematically rigorous fashion.

A. Frame independence of the EPH partition and the local flux

An important feature of the EPH partition is that it is *frame-independent* (*objective*), i.e., remains unchanged under time-dependent transformations of the form

$$\mathbf{x}=\mathbf{Q}(t)\mathbf{y}+\mathbf{a}(t), \tag{13}$$

where $\mathbf{y}$ denotes the new spatial variables, $\mathbf{Q}(t)$ is a proper orthogonal tensor, and $\mathbf{a}(t)$ is a smooth function of time. We show this, along with the frame independence of the local flux and $\varphi^{\pm}$, in Sec. 2 of the Appendix.

We recall that frame independence is a stronger invariance property than Galilean invariance, which would only require the partition to remain unchanged for time-independent $\mathbf{Q}$ and linear-in-time $\mathbf{a}(t)$. As a consequence of full frame independence, the EPH partition will remain unchanged even if one transforms the velocity field $\mathbf{v}$ from the fixed ''lab frame'' to a frame co-moving with the eigenvectors of $\mathbf{S}$ or other distinguished directions along a trajectory $\mathbf{x}(t)$. Previous attempts to capture Lagrangian hyperbolicity did not have this feature and hence gave different results in different coordinate systems (cf. Sec. V).

B. EPH partition and Lagrangian particle dynamics

In order to illuminate the significance of the EPH partition for Lagrangian mixing, we first need to fix some definitions about material structures in two-dimensional fluid flows. In the present context, a *material line* is a smooth time-dependent curve of fluid particles advected by the velocity field $\mathbf{v}(\mathbf{x},t)$. In a turbulent flow most material lines keep changing their stability type: for some time they might attract or repel particles, while at other times they may have a neutral stability type. In what follows we seek to find material lines that display the same stability type over a (potentially short) but fixed time interval $I=[t_0,t_1]$ with $t_1>t_0$.

We call a material line *repelling* over I if all infinitesimal perturbations transverse to it strictly increase throughout I.[35] A material line is said to be *attracting* over I if all infinitesimal perturbations transverse to it strictly decrease throughout I. We call a material line *hyperbolic* over I if it is either attracting or repelling over I. We will define two further classes of nonhyperbolic material lines (elliptic and parabolic) after we list our main theorems on hyperbolicity.

Note that the Lagrangian notions of hyperbolicity or nonhyperbolicity over a whole time interval are fundamentally different from their instantaneous Eulerian counterparts. Lagrangian hyperbolicity may remain completely hidden in instantaneous Eulerian snapshots of the velocity field (see, e.g., the examples in Sec. VI). Our main results below explore the relationship between frame-independent Eulerian features observed over an interval of time and Lagrangian hyperbolicity.

Theorem 1 (Sufficient condition for Lagrangian hyperbolicity): *Suppose that a trajectory* $\mathbf{x}(t)$ *does not leave the set* $\mathcal{H}(I)$. *Then* $\mathbf{x}(t)$ *is contained in a hyperbolic material line over I.*

The proof of the above statement turns out to be quite technical. One needs to employ a finite-time Lyapunov-function argument, combined with a lesser known topological technique, the Wasewsky principle. The proof also relies heavily on recently proven finite-time invariant manifold results from Haller.[24] Details can be found in Sec. 3 of the Appendix.

We stress that the above criterion for finite-time hyperbolicity is only sufficient. It may very well happen that hyperbolic material lines exist in the elliptic region $\mathcal{E}(t)$ (cf. Example 3 in Sec. VI). The result below describes necessary properties of hyperbolic material lines that ''stray'' out of the hyperbolic region $\mathcal{H}(I)$. To state this result, we define

$$\varphi_0(\mathbf{x},t)=\min(\varphi^+(\mathbf{x},t),\varphi^-(\mathbf{x},t)).$$

Note that φ_0 is positive in the hyperbolic region, zero in the parabolic region, and negative in the elliptic region.

Theorem 2 (Necessary condition for Lagrangian hyperbolicity): *Suppose that a trajectory* $\mathbf{x}(t)$ *is contained in a hyperbolic material line over I. Then*

(i) $\mathbf{x}(t)$ *can only intersect* $\mathcal{P}(I)$ *at isolated time instances.*

(ii) *If* $I_{\mathcal{E}}$ *denotes a time interval that the trajectory spends in* $\mathcal{E}(I)$, *then*

$$\int_{I_{\mathcal{E}}}|\varphi_0(\mathbf{x}(t),t)|dt<\frac{\pi}{2}.$$

The proof of this result can be found in Sec. 4 of the Appendix. Motivated by Theorem 2, we define *elliptic material lines* over I as nonhyperbolic material lines that either

stay in $\mathcal{E}(I)$ or stay in regions of zero strain over I [cf. Fig. 2(d)]. Our next theorem is concerned with the existence of such material lines.

Theorem 3 (Sufficient condition for Lagrangian ellipticity): *Suppose that a trajectory* $\mathbf{x}(t)$ *is contained in the set* $\mathcal{E}(I)$ *and*

$$\int_I |\varphi_0(\mathbf{x}(t),t)|dt \geqslant \frac{\pi}{2}. \tag{14}$$

Then $\mathbf{x}(t)$ *is contained in an elliptic material line over I.*

The proof of this theorem can be found in Sec. 5 of the Appendix.

We call a material line *parabolic* over I if $\mathbf{S}(t)$ is nonvanishing along it and all infinitesimal perturbations transverse to it stay constant in length throughout the interval I. The requirement of nonvanishing strain is meant to exclude elliptic material lines that simply rotate without any shear, like those shown in Fig. 2(d). One can think of parabolic material lines as those imbedded in a shear layer, displaying the neutral stability type. Based on our discussion at the end of Sec. III A, the only case in which this can happen is when $\mathbf{M}_Z$ remains positive semidefinite over a period of time. Therefore, we see the following result.

Theorem 4 (Sufficient and necessary condition for Lagrangian parabolicity): *A trajectory* $\mathbf{x}(t)$ *is contained in a parabolic material line over I if and only if it does not leave the set* $\mathcal{P}(I)$.

C. A dynamic condition for Lagrangian hyperbolicity

Our discussion of Lagrangian hyperbolicity and nonhyperbolicity has been purely kinematic: no use of the equations governing the evolution of the velocity field has been made. However, it would undoubtedly be of interest to interpret the criteria of Sec. IV B in dynamic terms that involve quantities from the governing equations. Here we consider the simplest case when the governing equations are just the two-dimensional incompressible Navier–Stokes equations. In that setting, we are able to obtain a mixed kinematic-dynamic sufficient condition for the existence of finite-time-hyperbolic material lines.

The key idea is to describe the hyperbolic region $\mathcal{H}(I)$ in dynamical terms and then reformulate Theorem 1 in these new terms. To this end, let us consider the Navier–Stokes equation

$$\frac{\partial \mathbf{v}}{\partial t} + (\mathbf{v}\cdot\nabla)\mathbf{v} = -\frac{1}{\rho}\nabla p + \nu\nabla^2\mathbf{u} + \mathbf{f},$$

where ρ denotes the density, p is the pressure, ν is the kinematic viscosity, and $\rho\mathbf{f}$ contains divergence-free body forces. We recall that for the Navier–Stokes equation, the material derivative of the rate of strain tensor satisfies the equation

$$\dot{\mathbf{S}} = -(\mathbf{S}^2 + \mathbf{\Omega}^2) - \frac{1}{\rho}\mathbf{P} + \nu\nabla^2\mathbf{S} + \mathbf{G}, \tag{15}$$

where $\mathbf{\Omega} = \frac{1}{2}(\nabla\mathbf{v} - \nabla\mathbf{v}^T)$ is the vorticity tensor, $P_{ij} = \partial^2 p/(\partial x_i \partial x_j)$ denotes the pressure Hessian, and $\mathbf{G} = \frac{1}{2}(\nabla\mathbf{f} + \nabla\mathbf{f}^T)$ is the symmetric part of the body force gradient.[32]

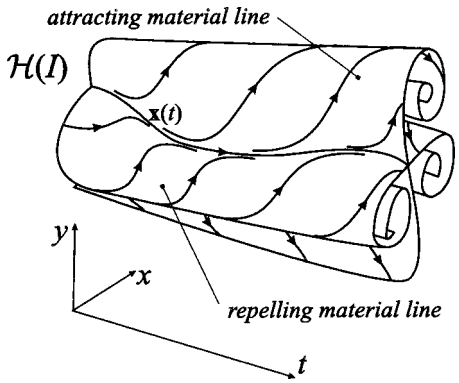

FIG. 4. Attracting and repelling material lines (finite-time unstable and stable manifolds) containing a trajectory $\mathbf{x}(t)$ that lies in the hyperbolic set $\mathcal{H}(I)$.

Let $s(\mathbf{x},t) \geqslant 0$ denote the largest eigenvalue of $\mathbf{S}(\mathbf{x},t)$, and let $\omega(\mathbf{x},t) = (\nabla \times \mathbf{u}(\mathbf{x},t))_z$ denote the z-component of the vorticity. Furthermore, let $\kappa(\mathbf{x},t)$ denote the largest eigenvalue of $\mathbf{P}(\mathbf{x},t)$, and let $\sigma(\mathbf{x},t) \geqslant 0$ and $\gamma(\mathbf{x},t) \geqslant 0$ denote the largest eigenvalues of $\nabla^2\mathbf{S}(\mathbf{x},t)$ and $\mathbf{G}(\mathbf{x},t)$, respectively. We can then prove the following result.

Theorem 5 (Sufficient dynamic condition for Lagrangian hyperbolicity): *Suppose that over a time interval I a fluid trajectory* $\mathbf{x}(t)$ *stays in the time-dependent physical region satisfying*

$$\left(s - \frac{|\omega|}{2}\right)^2 > \frac{1}{\rho}\kappa + \nu\sigma + \gamma. \tag{16}$$

Then $\mathbf{x}(t)$ *is contained in a hyperbolic material line over I.*

We prove this theorem in Sec. 6 of the Appendix. An inspection of the proof shows that Theorem 5 is a slightly weaker form of Theorem 1: its main condition may not be satisfied for some hyperbolic material lines that would normally be identified by Theorem 1. At the same time, it does offer a simple frame-independent relation between important kinematic and dynamic quantities that should be important in specific problems. For instance, in many applications, such as active flow control, one needs to go beyond identifying Lagrangian structures in a given velocity field: one actually aims to create, destroy, or shape such structures by altering dynamic features of the velocity field. According to the theorem above, mixing can be enhanced in a given region if the Eulerian condition (16) is satisfied on a large subset of the region for extended times. We shall not pursue this approach here but note that Theorem 1 should provide a good starting point.

In the following we discuss how our criteria on Lagrangian coherent structures can be used to isolate distinguished material structures in space–time that have a major impact on particle mixing. A class of these *Lagrangian coherent structures (LCS)* will act as barriers to mixing, while others will act as enhancers of mixing.

D. Hyperbolic LCS: Stretch and fold lines

Theorem 1 guarantees that all trajectories that remain in the hyperbolic set $\mathcal{H}(I)$ are contained in attracting and repelling material lines over the time interval I. The attracting

material lines act as finite-time unstable manifolds for the trajectory, while the repelling ones act as finite-time stable manifolds (see Fig. 4). As discussed in Haller,[24] such manifolds are not unique over finite time intervals: in general, there will be infinitely many material lines containing $\mathbf{x}(t)$, all behaving as stable and unstable manifolds for $\mathbf{x}(t)$. However, the distance between two possible finite-time stable or unstable manifolds tends to zero exponentially near $\mathbf{x}(t)$ as the length of the time interval I increases. Therefore, the stable and unstable manifolds of trajectories spending longer times in $\mathcal{H}$ become well-defined up to exponentially small uncertainties.

Trajectories lying inside the hyperbolic set $\mathcal{H}(I)$ will not be isolated: they will typically form open sets in space–time. Accordingly, there will be *infinitely many* repelling and attracting material lines (finite-time invariant manifolds) in the hyperbolic region. Out of this infinitely many, the most influential ones can be defined as hyperbolic Lagrangian coherent structures. One can quantify the influence of a hyperbolic material line on neighboring particles in at least three different ways, as we describe below. The first two of these definitions have already been suggested in relation with earlier frame-dependent approaches to Lagrangian hyperbolicity, and here we will only adjust them to our current setting.

Stretch lines can be defined as repelling material lines that stay in $\mathcal{H}$ for locally the longest or shortest time in the flow. Similarly, *fold lines* can be defined as attracting material lines that stay in $\mathcal{H}$ for locally the longest or shortest time in the flow. In practical terms, one identifies such lines at $t=t_0$ as local extremum curves of the hyperbolicity time field (cf. Haller and Yuan[25])

$$\tau_h(t_0,\mathbf{x}_0)=\int_{\{t\in\mathcal{I}|\mathbf{x}(t)\in\mathcal{H}(t)\}} dt. \tag{17}$$

Alternatively, stretch and fold lines can be defined as material lines along which the time integral of the local flux is maximal or minimal. By (ii) of Theorem 1, one can locate hyperbolic LCS at $t=t_0$ by looking for local extremum curves of the scalar field,

$$\sigma(t_0,\mathbf{x}_0)=\int_{\{t\in\mathcal{I}|\mathbf{x}(t)\in\mathcal{H}(t)\}} |\mathbf{S}(\mathbf{x}(t),t)|dt. \tag{18}$$

In the context of a possible improvement to the result of Haller and Yuan,[25] this scalar field was proposed by Lapeyre *et al.*[26] as a relevant indicator of hyperbolic Lagrangian coherent structures. We note that if the largest strain eigenvector along $\mathbf{x}(t)$ were tangent to the folding line containing $\mathbf{x}(t)$, then $\sigma(t_0,\mathbf{x}_0)/t$ would coincide with the finite-time Lyapunov exponent field calculated for the initial condition $\mathbf{x}_0$. However, such a special orientation of the strain eigenvectors occurs with probability zero due to the presence of shear and rotation in the flow (see, e.g., Pierrehumbert and Yang[19]).

The difference between the two scalar fields above is that τ_h will be sensitive to all stretch and fold lines regardless of their strength of hyperbolicity, while σ will effectively capture the strongest such structures, i.e., the ones that correspond to high levels of strain. When implemented numerically, both scalar fields are locally maximized by *stretch lines in forward time calculations* and *fold lines in backward time calculations.* The reason is that particles near stretching lines spend longer time in hyperbolic regions that those near folding lines. As a simple analogy, one can picture a saddle point: along its stable manifold, i.e., a stretch line, particles spend a long time before they leave the vicinity of the saddle along its unstable manifold, a fold line.

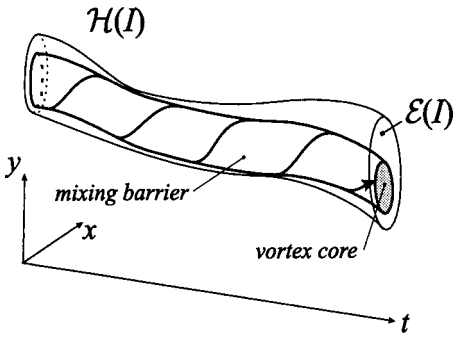

FIG. 5. Mixing barrier formed by a closed, material line that stays in the elliptic set for a long enough time.

A third way to localize stretch and fold lines turns out to be plotting the following time-dependent field:

$$\mu(t,t_0,\mathbf{x}_0)=\begin{cases} |\mathbf{S}(\mathbf{x}(t),t)|, & \text{if} \quad \mathbf{x}(t)\in\mathcal{H}(t), \\ 0, & \text{if} \quad \mathbf{x}(t)\notin\mathcal{H}(t). \end{cases}$$

Note that μ is nothing else but the instantaneous value of the local flux for instantaneously hyperbolic particles, while it is zero for instantaneously elliptic particles. As we show in Sec. VII, this field is particularly effective in reconstructing stretching and folding lines from short-time velocity data. The lines will appear as local *minimizers* of this field as particles very close to stretching lines tend to accumulate near folding lines and then spiral into an elliptic region of a nearby eddy (see Fig. 4). Since this scenario is typical in two-dimensional turbulence, $\mu(t,\mathbf{x}_0)$ appears to be a fast-converging indicator of long-lived stretching lines in forward time and folding lines in backward time.

We finally note that stretching and folding lines will generally have finite thickness as they can only be expected to be unique curves in infinite-time velocity fields. However, just as attracting or repelling material lines, the more time they spend in the hyperbolic region the thinner they become.

E. Elliptic LCS: Vortex cores

A consequence of Theorem 3 is the following: while trajectories in a finite-time hyperbolic material line can enter the elliptic set $\mathcal{E}(I)$, they can only stay there for short times. What ''short time'' means locally in the flow is determined by the inequality (14). The length of the time interval for which the inequality turns into an equality can be considered an upper estimate for $T^*/4$, where T^* denotes the local eddy turnover time.

By our results, elliptic material lines do not experience exponential stretching or folding over the time interval I. Picking the maximal (smooth) closed material line that stays

in a given component of the elliptic set $\mathcal{E}(I)$, we therefore obtain a barrier to mixing. In the extended phase space of $(\mathbf{x},t)$, this barrier can be pictured as an invariant cylinder (see Fig. 5). While the $t=$const cross section of such a cylinder may deform, its area is preserved by incompressibility. The existence of these cylinders explains the old observation that vortices in two-dimensional turbulence admit impenetrable vortex cores (see, e.g., Elhmaïdi *et al.*[5]).

The above cylinders are the generalizations of KAM tori from time-periodic velocity fields. Note that the existence of invariant cylinders in an arbitrary velocity field is a trivial result: *any* smooth closed material line generates an invariant cylinder in the extended phase space. What is special about time-periodic velocity fields is that certain closed material curves give rise to cylinders that are actually *periodic in time*: such time-periodic cylinders form the well-known KAM tori when time is viewed as a periodic variable.

In a velocity field with general time dependence one cannot expect to find periodic-in-time cylinders in the extended phase space. A randomly picked closed material curve will generate a cylinder, but its cross section will typically undergo exponential stretching and folding. The cylinders we identified above do not stretch intensely, and hence keep particles confined to their interiors, the vortex cores.

In practical terms, elliptic LCS at $t=t_0$ can be defined as open sets on which the *ellipticity time field,*

$$\tau_e(t_0,\mathbf{x}_0)=\int_{\{t\in\mathcal{I}|\mathbf{x}(t)\in\mathcal{E}(t)\}} dt,$$

is locally maximal. The scalar field $\tau_e(t_0,\mathbf{x}_0)$ can be computed and then interpolated from a grid of initial conditions for any fixed initial time $\mathbf{x}_0$.

It remains to note that in very special velocity fields some elliptic material lines can become unstable due to resonances. Such a situation is atypical in turbulent flows: it would require sustained near-periodic and near-resonant time dependence around trajectories forming the material lines. However, even if such flow conditions arise, the resulting instability generically remains contained.[36] For completeness, we discuss a related example (originally proposed by Pierrehumbert and Yang[19]) in Sec. VI.

F. Parabolic LCS: Shear jets

The third kind of basic Lagrangian coherent structure we can identify from our theorems is a *shear jet:* a set of fluid trajectories that travel in the parabolic region $\mathcal{P}(I)$ over some time interval I. Material lines in this set may ''slide'' on each other, but they do not repel or attract fluid particles at a noticeable rate over finite time intervals. While the material lines forming the jet are locally parallel, the jet as a whole may rotate (see Fig. 6). As an example one can think of a two-dimensional, inviscid channel flow where the channel rotates within the $x-y$ plane. As we noted earlier, the occurrence of such a structure in a general turbulent flow is unlikely since there is no *a priori* reason why the strain acceleration tensor would admit a single zero eigenvalue over a whole region. A notable exception would be a laminar shear flow near a boundary with no-flow boundary condition.

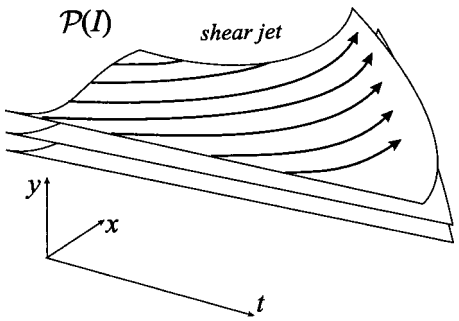

FIG. 6. Schematic view of material lines forming a shear jet in space–time.

V. RELATIONSHIP TO EULERIAN PARTITIONS OF 2-D TURBULENCE

Here we compare the EPH partition to two instantaneous partitions of two-dimensional turbulence that have been suggested and used in the literature. Both partitions are essentially based on short-time approximations of particle dynamics and assume slowly varying properties of the velocity field.

A. The Okubo–Weiss partition

The Okubo–Weiss partition identifies elliptic regions for the velocity field $\mathbf{v}(\mathbf{x},t)$ at time t as spatial domains satisfying $\det(\nabla\mathbf{v}(\mathbf{x},t))>0$ (see Okubo[37] and Weiss[38]). Hyperbolic regions are defined as those where $\det(\nabla\mathbf{v}(\mathbf{x},t))<0$. Using the positive eigenvalue s of $\mathbf{S}$ and the vorticity $\omega=|\nabla\times\mathbf{v}|$, the above criterion can be phrased as $s^2-\omega^2/4<0$ for the elliptic region, and $s^2-\omega^2/4>0$ for the hyperbolic region. This criterion is essentially an attempt to decide whether the $\boldsymbol{\xi}=\mathbf{0}$ solution of the linearized equation (6) is hyperbolic (i.e., of saddle type) or elliptic (i.e., of center type). The Okubo–Weiss criterion would give the exact answer to this question if $\mathbf{A}(t)=\nabla\mathbf{v}(x(t),t)$ were a time-independent matrix: in that case the sign of $\det(\mathbf{A})$ could indeed be used to find the stability type of $\boldsymbol{\xi}=\mathbf{0}$.[39] However, $\mathbf{A}(t)$ has explicit time dependence even for steady flows, in which case the eigenvalues of $\mathbf{A}(t)$, in general, do not have any meaning for the stability type of $\mathbf{x}(t)$ (see, e.g., Verhulst[40] or Hale[41] for counterexamples and further references). One still hopes that if $\mathbf{A}(t)$ is slowly varying then its eigenvalues remain relevant indicators of stability. This was found to be the case near stagnation points in numerical simulations by Basdevant and Philipovitch.[42]

Recently, Haller and Yuan[25] gave a rigorous bound for the speed of rotation of the eigenvectors of $\mathbf{A}(t)$ below which $\det(\nabla\mathbf{v}(\mathbf{x},t))<0$ indeed implies finite-time hyperbolicity for $\mathbf{x}(t)$. This ''$\alpha-\beta$ criterion'' gives a Galilean invariant but frame-dependent partition of 2-D turbulence into regions that are known to be exactly hyperbolic and regions whose stability type remains undecided. A three-dimensional extension of this result was given in Haller.[27] More recently, Lapeyre *et al.*[26] proposed that applying the $\alpha-\beta$ criterion in a strain basis would give an improved sufficient condition for finite-time hyperbolicity. However, the frame dependence of the $\alpha-\beta$ criterion combined with the numerical errors due

to the calculation $\nabla \mathbf{v}$ in a rotating frame actually gives similar or somewhat weaker results in a strain basis for most flow fields (see Haller[43]).

B. The Okubo–Weiss partition in strain basis

A more refined way to study the exact stability type of the origin in (6) is to factor out the part of the time dependence of $\mathbf{A}(t)$ that comes from the rotation of the eigenvectors of its symmetric part, the rate-of-strain tensor. This approach was first pursued by Dresselhaus and Tabor,[44] who derive the analog of Eq. (6) in the strain basis (see also Dritschel *et al.*[45] for a similar approach in the framework of a specific problem). In terms of our notation, the resulting equation can be written as

$$\dot{\boldsymbol{\xi}} = \mathbf{A}_{\text{strain}}(t)\,\boldsymbol{\xi}, \tag{19}$$

with

$$\mathbf{A}_{\text{strain}} = \mathbf{Q}^T\mathbf{A}\mathbf{Q} - \mathbf{Q}^T\dot{\mathbf{Q}} = \boldsymbol{\Sigma} + (\mathbf{Q}^T\boldsymbol{\Omega}\mathbf{Q} - \mathbf{Q}^T\dot{\mathbf{Q}}). \tag{20}$$

Here $\boldsymbol{\Sigma}(t)$ is a diagonal matrix containing the eigenvalues of $\mathbf{S}(t)$, $\boldsymbol{\Omega}(t)$ denotes the skew-symmetric part of $\mathbf{S}(t)$, and $\mathbf{Q}(t)$ is a proper orthogonal matrix containing the normalized eigenvectors of $\mathbf{S}(t)$. Taking this approach further, Tabor and Klapper[32] propose to assess the instantaneous stability of (19) by applying the Okubo–Weiss criterion to it. More concretely, using the notation $\pm(\omega - \omega')/4$ for the off-diagonal terms of the skew-symmetric part of $\mathbf{A}_{\text{strain}}$, they distinguish between ''local rotation domination'' characterized by

$$s^2 - (\omega - \omega')^2 < 0 \Leftrightarrow \det(\mathbf{A}_{\text{strain}}) > 0, \tag{21}$$

and ''local strain domination'' characterized by

$$s^2 - (\omega - \omega')^2 > 0 \Leftrightarrow \det(\mathbf{A}_{\text{strain}}) < 0. \tag{22}$$

Of course, this criterion is still formal since $\mathbf{A}_{\text{strain}}$ remains time dependent and hence its eigenvalues cannot be used directly to argue about the stability of $\mathbf{x}(t)$ (see, however, Dresselhaus and Tabor[44] for a few simple cases when they *can* be).

The above partition will only be relevant to the actual stability of fluid trajectories if one assumes that $\mathbf{A}_{\text{strain}}(t)$, the velocity gradient expressed in the strain basis, is slowly varying in some sense.[46] This view is taken by Lapeyre *et al.*[47] in an equivalent derivation of the same partition (see also Klein *et al.*[48]). This latter derivation aims to find alignment directions for tracer gradients and vorticity in two-dimensional turbulence. Along a trajectory the gradient of a nondiffusive passive tracer, $\nabla q(\mathbf{x}(t),t)$, solves the linear differential equation $\dot{\boldsymbol{\eta}} = -\mathbf{A}^T(t)\boldsymbol{\eta}$. Lapeyre *et al.* transform this equation to the strain basis then consider the ''adiabatic limit,'' i.e., ignore the time dependence of the transformed coefficient matrix $-\mathbf{A}^T_{\text{strain}}(t)$. They then proceed to find the asymptotic direction of any initial tracer gradient by formally solving the resulting constant-coefficient ODE. However, one can actually predict the result without solving the ODE: an adiabatic alignment direction will exist precisely if $\boldsymbol{\eta} = \mathbf{0}$ is a saddle point for the ''frozen-time'' ODE. In that case any initial tracer gradient will approach the unstable manifold of the saddle exponentially fast. Thus a formal alignment direction can be found whenever $-\mathbf{A}^T_{\text{strain}}$ has real eigenvalues, which amounts to the requirement that $\det(-\mathbf{A}^T_{\text{strain}}) < 0$. Since

$$\det(-\mathbf{A}^T_{\text{strain}}) = \det(\mathbf{A}^T_{\text{strain}}) = \det(\mathbf{A}_{\text{strain}}),$$

a formal alignment direction exists precisely when (22) is satisfied. Lapeyre *et al.* call the region of the flow obeying (21) and (22) ''effective rotation dominated,'' and ''strain dominated,'' respectively, and refer to the boundary between the two regions ($\det \mathbf{A}_{\text{strain}} = 0$) as ''strain-effective rotation compensated'' region. In the recent work of Lapeyre *et al.*[49] the significance of this partition for the alignment of diffusive tracer gradients is explored.

Inferring actual Lagrangian stability or tracer gradient alignment from the partition (21)–(22) is not a rigorous procedure: it is based on a somewhat vague ''frozen-time'' assumption. Even if writing $\mathbf{A}_{\text{strain}}(\epsilon t)$ were correct for some small parameter ϵ, the lack of periodic time dependence for $\mathbf{A}_{\text{strain}}$ would prevent one from applying classic averaging techniques to justify a passage to the adiabatic (frozen-time) limit. Nevertheless, (21)–(22) turn out to be formally related to the EPH partition that we derived in the previous section. In particular, the instantaneous elliptic region $\mathcal{E}(t)$ coincides with the set defined as $\det(-\mathbf{A}^T_{\text{strain}}(t)) > 0$, and the region $\mathcal{H}(t)$ coincides with the set defined as $\det(-\mathbf{A}^T_{\text{strain}}(t)) < 0$. This can be seen from Fig. 2: the geometry depicted in Fig. 2(a) implies that origin is an instantaneous saddle point for the linearized equation (6) in strain basis, while the geometry of Fig. 2(b) is only possible if the origin is an instantaneous center for the linearized flow. The difference between our approach and formal derivations of (21)–(22) is that ours leads to rigorous analytic criteria for Lagrangian hyperbolicity or nonhyperbolicity withoutassuming adiabatic features or passage to a different basis.

VI. EXAMPLES

The examples below show the use of our theorems on hyperbolic and nonhyperbolic material surfaces for linear time-dependent velocity fields. In Examples 1–3 we selected velocity fields that are exactly solvable and hence the predictions of Theorems 2–4 can be verified. Even these simple examples, however, highlight the difference between instantaneous Eulerian predictions and actual Lagrangian hyperbolicity. Example 4 is a time-dependent velocity field proposed by Pierrehumbert and Yang[19] for which explicit solutions are not known.

Example 1: The first example below shows how the EPH partition can rigorously identify Lagrangian hyperbolic behavior when the Okubo–Weiss criterion or the $\alpha - \beta$ criterion of Haller and Yuan[25] fail to indicate hyperbolicity.

Consider the incompressible velocity field $\mathbf{v}(\mathbf{x},t) = \mathbf{A}(t)\mathbf{x}$ with

$$\mathbf{A}(t) = \begin{pmatrix} \sin 2\omega t & \omega + \cos 2\omega t \\ -\omega + \cos 2\omega t & -\sin 2\omega t \end{pmatrix}.$$

This is just the velocity field of a uniform strain field $\dot{x} = y$, $\dot{y} = x$ transformed to a frame that is uniformly rotating

with angular velocity ω. As a result, we know that the origin $\mathbf{x}=0$ is finite-time hyperbolic on any finite time interval.

However, applying the Okubo–Weiss principle or its rigorous Lagrangian version from Haller and Yuan,[25] we cannot recover the hyperbolicity of the origin if $\det(\mathbf{A})=\omega^2-1>0$, i.e., the speed of the rotation for the frame reaches $\omega^*=1$.

The explicit evaluation of the Okubo–Weiss criterion in strain basis is computational: it requires the calculation of the derivatives of the eigenvectors of the symmetric part of $\mathbf{A}(t)$. In contrast, the strain acceleration tensor is easily found to be

$$\mathbf{M}=\dot{\mathbf{S}}+2\mathbf{S}\mathbf{A}=\begin{pmatrix}2 & 0\\ 0 & 2\end{pmatrix}.$$

Since $\mathbf{M}$ is positive definite on the whole plane, its restriction $\mathbf{M}_Z$ to the zero strain set Z must also be positive definite, thus $\mathbf{x}=\mathbf{0}$ lies in the hyperbolic set $\mathcal{H}(I)$ for any time interval I. Then Theorem 1 guarantees the finite-time hyperbolicity of the origin over any finite time interval.

Example 2: The following example shows that the positive definiteness of $\mathbf{M}_Z$ cannot be replaced by the positive definiteness of $\mathbf{M}$ in the definition of the hyperbolic region $\mathcal{H}(t)$.

Let us consider a linear velocity field of the form $\mathbf{v}(\mathbf{x},t)=\mathbf{A}(t)\mathbf{x}$ with

$$\mathbf{A}(t)=\begin{pmatrix}\lambda(t) & 0\\ 0 & -\lambda(t)\end{pmatrix},$$

where $\lambda(t)>0$ for all t. Direct integration shows that the origin is linearly unstable, and hence it is finite-time hyperbolic on any finite time interval. The strain acceleration tensor is of the form

$$\mathbf{M}=\begin{pmatrix}\dot{\lambda}+2\lambda^2 & 0\\ 0 & -\dot{\lambda}+2\lambda^2\end{pmatrix}.$$

Note that $\mathbf{M}$ will only be a positive definite matrix for $|\dot{\lambda}|<2\lambda^2$, i.e., if λ changes slowly enough. However, Theorem 1 only requires $\mathbf{M}$ to be positive definite on the zero set Z of $\langle\boldsymbol{\xi},\mathbf{S}\boldsymbol{\xi}\rangle$ for the origin to lie in an attracting (as well as on a repelling) material line. In this example we have

$$\boldsymbol{\xi}^{\pm}(t)=\begin{pmatrix}1\\ \pm 1\end{pmatrix},$$

and hence

$$\mathbf{M}_Z(\boldsymbol{\xi})=\langle\boldsymbol{\xi},\mathbf{M}\boldsymbol{\xi}\rangle|_Z=4\lambda^2|\boldsymbol{\xi}|^2.$$

Therefore, $\mathbf{M}_Z$ is positive definite and Theorem 1 correctly predicts the finite-time hyperbolicity of the origin for any smooth function $\lambda(t)>0$.

Example 3: This example shows how Theorem 3 can be used to exclude finite-time Lagrangian ellipticity even if the formal application of the Okubo–Weiss criterion in strain basis incorrectly suggests ellipticity (or "effective rotation domination").

Consider the incompressible velocity field $\mathbf{v}(\mathbf{x},t)=\mathbf{A}(t)\mathbf{x}$ with

$$\mathbf{A}(t)=\begin{pmatrix}-1 & 2a(t)\\ 0 & 1\end{pmatrix},$$

where the function $a(t)$ is to be specified later. One can directly integrate the ODE $\dot{\mathbf{x}}=\mathbf{v}(\mathbf{x},t)$ to obtain the solution

$$\mathbf{x}(t)=\begin{pmatrix}e^{-(t-t_0)} & 2\int_{t_0}^{t}e^{2\tau-t-t_0}a(\tau)\,d\tau\\ 0 & e^{t-t_0}\end{pmatrix}\mathbf{x}_0,$$

where $\mathbf{x}_0$ is the initial position of the trajectory $\mathbf{x}(t)=(x(t),y(t))^T$ at time t_0. The $\mathbf{x}=\mathbf{0}$ trajectory is clearly finite-time hyperbolic for all times and is contained in the repelling material line (stable manifold) $y=0$. Below will show how different approaches to detecting Lagrangian hyperbolicity bear on this example.

Applying the Okubo–Weiss criterion gives $\det\mathbf{A}(t)=-1$, i.e., all trajectories are instantaneously Okubo–Weiss hyperbolic. To confirm actual Lagrangian hyperbolicity in the "lab frame" rigorously, we use the $\alpha-\beta$ criterion of Haller and Yuan.[25] This criterion ensures finite-time hyperbolicity on a finite-time interval $\mathcal{I}$ if

$$\alpha\lambda_{\min}>(2+\sqrt{2})\beta, \tag{23}$$

where $\lambda_{\min}$ denotes the minimum of the positive eigenvalue of $\mathbf{A}(t)$ over $\mathcal{I}$, α denotes the minimum of the norm of the determinant of a matrix $\mathbf{T}(t)$ containing the normalized eigenvectors of $\mathbf{A}(t)$ over $\mathcal{I}$, and β denotes the maximum of the norm $\dot{\mathbf{T}}(t)$ over $\mathcal{I}$. One calculates these quantities to find that (23) takes the form

$$\min_{t\in I}\frac{1}{\sqrt{a^2+1}}>\max_{t\in I}\frac{(2+\sqrt{2})\sqrt{[\dot{a}(a^2+1)-a^2]^2+a^2}}{\sqrt{(a^2+1)^3}}. \tag{24}$$

Therefore, if $a(t)$ varies slowly enough to obey the above bound on its derivative, finite-time hyperbolicity is guaranteed by the $\alpha-\beta$ criterion.

To evaluate the Okubo–Weiss criterion in strain basis, we would have to evaluate the formula (20) to determine the sign of $\det(\mathbf{A}_{\text{strain}}(t))$. This calculation is a tedious exercise and will be omitted here. Instead, the two components of the zero strain set and the strain acceleration tensor [cf. (3) and (4)] are easily found to be

$$\boldsymbol{\xi}^{\pm}=\begin{pmatrix}1\\ -a\pm\sqrt{a^2+1}\end{pmatrix},\quad \mathbf{M}=\begin{pmatrix}2 & \dot{a}-2a.\\ \dot{a}-2a & 4a^2+2\end{pmatrix}.$$

This in turn gives

$$\langle\boldsymbol{\xi}^{+},\mathbf{M}\boldsymbol{\xi}^{+}\rangle=2+(a+\sqrt{a^2+1})[2(2a-\dot{a})+2(2a^2+1)\times(a+\sqrt{a^2+1})],$$

$$\langle\boldsymbol{\xi}^{-},\mathbf{M}\boldsymbol{\xi}^{-}\rangle=2+(a-\sqrt{a^2+1})[2(2a-\dot{a})+2(2a^2+1)\times(a-\sqrt{a^2+1})].$$

According to our discussion in Sec. V B,

$$\det(\mathbf{A}_{\text{strain}})>0\Leftrightarrow\langle\boldsymbol{\xi}^{+},\mathbf{M}\boldsymbol{\xi}^{+}\rangle\langle\boldsymbol{\xi}^{-},\mathbf{M}\boldsymbol{\xi}^{-}\rangle<0, \tag{25}$$

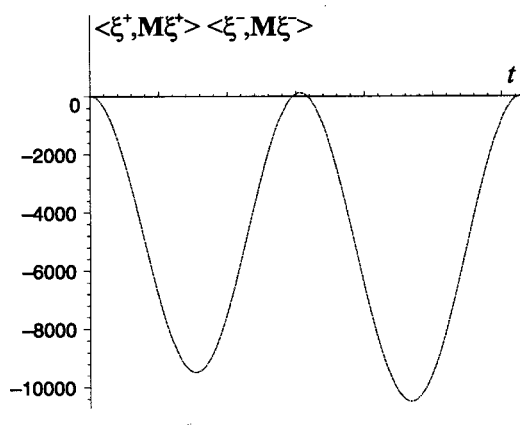

FIG. 7. The product $\langle \boldsymbol{\xi}^+, \mathbf{M}\boldsymbol{\xi}^+ \rangle \langle \boldsymbol{\xi}^-, \mathbf{M}\boldsymbol{\xi}^- \rangle$ as a function of time for Example 3.

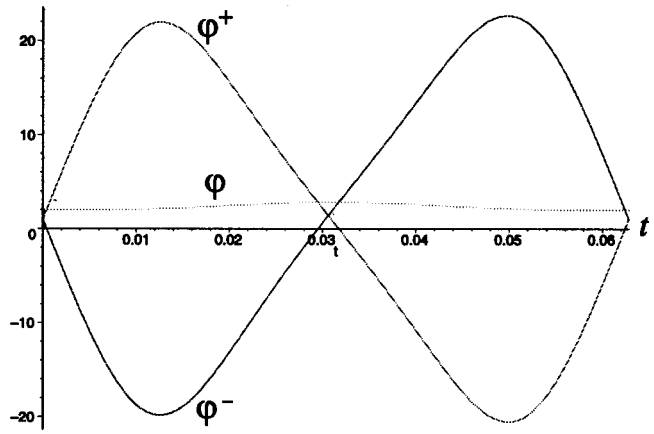

FIG. 8. The local flux φ and its two components φ^+ and φ^- for Example 3.

$$\det(\mathbf{A}_{\text{strain}}) < 0 \Leftrightarrow \langle \boldsymbol{\xi}^+, \mathbf{M}\boldsymbol{\xi}^+ \rangle \langle \boldsymbol{\xi}^-, \mathbf{M}\boldsymbol{\xi}^- \rangle > 0.$$

We now select $a(t) = (\sin 50t)^2$ which violates the finite-time hyperbolicity condition obtained in (24). For this choice of $a(t)$, we show $\langle \boldsymbol{\xi}^+, \mathbf{M}\boldsymbol{\xi}^+ \rangle \langle \boldsymbol{\xi}^-, \mathbf{M}\boldsymbol{\xi}^- \rangle$ as a function of time over one period of $a(t)$ in Fig. 7. Note that $\langle \boldsymbol{\xi}^+, \mathbf{M}\boldsymbol{\xi}^+ \rangle \times \langle \boldsymbol{\xi}^-, \mathbf{M}\boldsymbol{\xi}^- \rangle$ is predominantly negative apart from barely visible short positive intervals. By (21)–(22) and (25), the Okubo–Weiss criterion in the strain basis predicts predominant ellipticity near the trajectory $\mathbf{x} = \mathbf{0}$. In a fully numerical calculation of the criterion one would likely discount the short and weak Okubo–Weiss hyperbolic intervals as numerical errors. This is an example of how the original Okubo–Weiss criterion might accidentally perform much better in the lab frame than in the strain basis. This further underlines the fact that both versions of the criterion are based on nonrigorous calculations and hence can produce misleading results.

To evaluate the mathematically exact results we have derived in this paper, we first note that Theorem 1 immediately guarantees finite-time hyperbolicity over the short negative intervals where trajectories travel in $\mathcal{H}(t)$. For the rest of the time, trajectories are travelling in the elliptic region $\mathcal{E}(t)$, with the exception of the isolated times when they hit the parabolic region $\mathcal{P}(t)$ upon passing between $\mathcal{H}(t)$ and $\mathcal{E}(t)$. To avoid finite-time hyperbolicity, trajectories would have to spend long enough times in $\mathcal{E}(t)$ by Theorem 3. The two intervals over which trajectories are in $\mathcal{E}(t)$ are given by

$$I_1 = [0.0040, 0.0295],\ I_2 = [0.0317, 0.0624].$$

Figure 8 shows the graphs of the local flux components φ^+ and φ^-, as well as that of the total local flux φ, over one period of $a(t)$. We used high-precision numerical integration to obtain

$$\int_{I_1} |\varphi^+(\mathbf{x}(t),t)| + |\varphi^-(\mathbf{x}(t),t)| dt = 0.7528 < \pi,$$

$$\int_{I_2} |\varphi^+(\mathbf{x}(t),t)| + |\varphi^-(\mathbf{x}(t),t)| dt = 0.8157 < \pi,$$

for all trajectories, which implies $\int_{I_i} |\varphi_0(\mathbf{x}(t),t)| < \pi/2$. Therefore, trajectories always leave the elliptic region $\mathcal{E}(t)$ well before finite-time ellipticity would follow from Theorem 3. Thus true Lagrangian ellipticity cannot be concluded over the intervals I_1 and I_2 in spite of the fact that it is (incorrectly) suggested by the Okubo–Weiss criterion in strain basis.

Example 4: As our final example, we consider a time-dependent linear velocity field proposed by Pierrehumbert and Yang.[19] This velocity field will illustrate the power of our results on a problem in which explicit solutions for fluid trajectories are not available.

Consider the incompressible velocity field $\mathbf{v}(\mathbf{x},t) = \mathbf{A}(t)\mathbf{x}$ with

$$\mathbf{A}(t) = \begin{pmatrix} a(t) & 1 \\ -1 & -a(t) \end{pmatrix},$$

with some smooth function $a(t)$. If $a(t)$ is not constant in time, the nonzero solutions of this system are not known. Since $\det \mathbf{A}(t) = 1 - a^2(t)$, the Okubo–Weiss criterion predicts elliptic stability for the fixed point $\mathbf{x} = \mathbf{0}$ for $|a(t)| < 1$, and then hyperbolic stability type for $|a(t)| > 1$.

To obtain rigorous statements about Lagrangian hyperbolicity or nonhyperbolicity in this example, we first note that

$$\mathbf{S}(t) = \begin{pmatrix} a(t) & 0 \\ 0 & -a(t) \end{pmatrix},$$

$$\mathbf{M}(t) = \begin{pmatrix} \dot{a}(t) + 2a^2(t) & 2a(t) \\ 2a(t) & -\dot{a}(t) + 2a^2(t) \end{pmatrix},$$

$$\boldsymbol{\xi}^{\pm}(t) = \begin{pmatrix} 1 \\ \pm 1 \end{pmatrix},$$

which give

$$\langle \boldsymbol{\xi}^+, \mathbf{M}\boldsymbol{\xi}^+ \rangle \langle \boldsymbol{\xi}^-, \mathbf{M}\boldsymbol{\xi}^- \rangle = 16a^2(t)[a^2(t) - 1].$$

Then our Theorem 1 guarantees finite-time hyperbolicity for the origin (and for all other trajectories) over a time interval

I if $|a(t)|>1$ for all $t\in I$. Note that this is a highly nontrivial result since the trajectories of this time-dependent velocity field are not known explicitly.

If $a(t)$ is such that $|a^2(t)|<1$ holds on a finite-time interval I, then all trajectories are contained in the elliptic region $\mathcal{E}(I)$. The two local flux components are given by

$$\varphi^{\pm}(t)=(a^2\pm a)/|a| \tag{26}$$

along all trajectories. Recall that Theorem 2 only allows the origin to be finite-time hyperbolic over I if $\int_I|\varphi_0(t)|dt<\pi/2$, or equivalently,

$$\int_I 1-|a(t)|dt<\pi/2.$$

This last condition can be rewritten as

$$\int_I|a(t)|dt<I-\pi/2, \tag{27}$$

so we obtain that the origin (or any other trajectory of the velocity field) is automatically finite-time hyperbolic over time intervals that are shorter than $\pi/2$. However, no small perturbation to the fixed point $\mathbf{x}=\mathbf{0}$ can grow monotonically over long I intervals. A more precise estimate for the admissible length of finite-time hyperbolicity intervals can be obtained by evaluating the integral in (27) for a given choice of $a(t)$.

Using Theorem 3 and Eq. (26), we also conclude that for $|a^2(t)|<1$, all material lines are elliptic over time intervals I satisfying

$$\int_I|a(t)|dt\leqslant I-\pi/2.$$

By definition, elliptic material lines are contained in the elliptic region $\mathcal{E}(I)$, i.e., the basic flow geometry around them is rotational. Also by definition, they are not finite-time hyperbolic over I: infinitesimal perturbations to them may grow monotonically over subintervals of I, but the growth periods will be followed by periods of decay. Using the method of averaging, Pierrehumbert and Yang[19] showed that if $a(t)$ is periodic and small enough in norm, then the growth periods may dominate on average and lead to an overall instability of the origin. This occurs if the period of $a(t)$ is nearly commensurate with 2π, i.e., a resonance occurs between $a(t)$ and the periodic orbits of the $a(t)\equiv 0$ limit. This case gives an example of the resonant elliptic material lines mentioned at the end of Sec. IV E. The unbounded growth of perturbations to the $\mathbf{x}=0$ trajectory is the result of the interplay between two degenerate features that do not occur in general turbulent velocity fields. The first one is the periodic time dependence of the velocity field.[50] The second one is the linear nature of $\mathbf{v}$ that ''locks'' all trajectories in resonance for all times. In contrast, generic nonlinear velocity fields admit resonance regions that are localized in space.[36]

VII. NUMERICAL EXPERIMENTS ON BAROTROPIC TURBULENCE

In this section we reconsider the numerical experiments performed in Haller and Yuan[25] and show how a complete map of stretching lines, folding lines, and regions of no mixing can be extracted from the data set with high precision. We consider the quasigeostrophic vorticity equation,

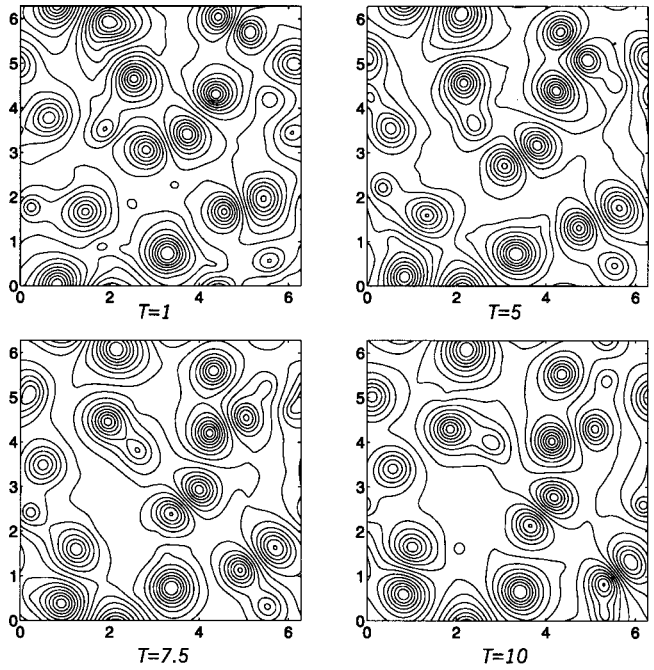

FIG. 9. Instantaneous contour plots of the potential vorticity showing robust (Eulerian) coherent structures.

$$\frac{\partial q}{\partial t}+[\psi,q]=-\nu_4\nabla^4 q, \tag{28}$$

with hyperviscosity $\nu_4=5\times 10^{-7}$. The quasigeostrophic potential vorticity q is defined as $q=\nabla^2\psi-\gamma^2\psi$, with $\psi(x,y,t)$ denoting the nondimensionalized free surface (stream function). The constant γ is the scaled inverse of the Rossby deformation radius. Following Provenzale *et al.*,[28] we select $\gamma=10$ to ensure the presence relatively robust coherent structures. Equation (28) is solved on the square domain $(0,2\pi)^2$, with 128×128 resolution and with a random Gaussian distribution of vorticity, using the pseudo-spectral code employed in Provenzale *et al.*[28] After an initial start-up period, robust Eulerian coherent structures emerge, as evidenced by the contour plots of q shown in Fig. 9. For our analysis below we saved snapshots of the velocity field that were $\Delta t=0.1$ apart over the time interval $\mathcal{I}=[5,9]$. We also saved the position of particles released from a uniform initial grid of 256×256. The Okubo–Weiss criterion and its Lagrangian version, the $\alpha-\beta$ criterion, were evaluated in Haller and Yuan[25] for this simulation and will be omitted here. Instead, we use the EPH partition and our theorems from Sec. IV B to search for different Lagrangian coherent structures. In this open turbulent flow parabolic structures are nongeneric, thus our discussion will be limited to stretching and folding lines and vortex cores.

As we noted in Sec. IV D, Lagrangian coherent structures can be defined as material lines that are locally the most influential in mixing. This influence can be quantified in several ways. We first plot the hyperbolicity time field $\tau_h(5,\mathbf{x}_0)$ and the ellipticity time field $\tau_e(5,\mathbf{x}_0)$ in Fig. 10 based on a

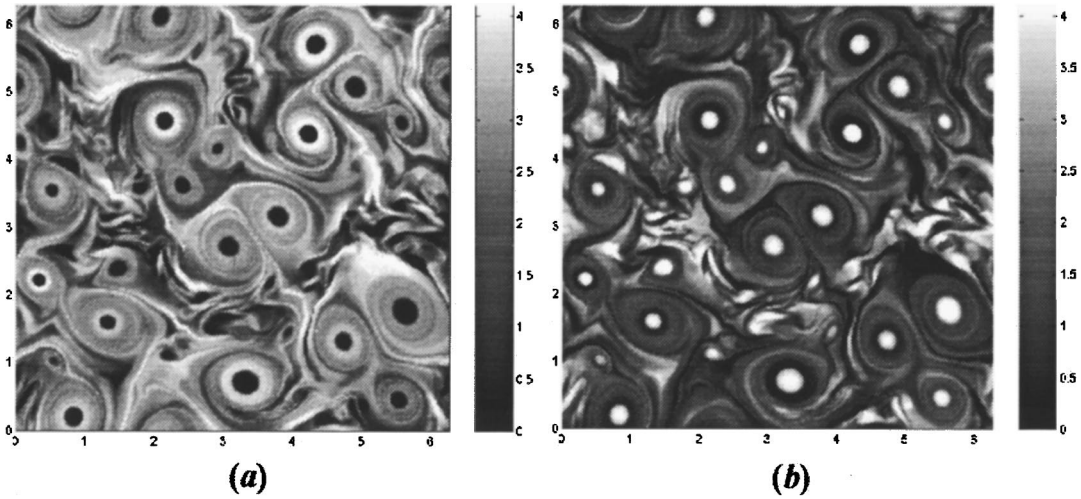

FIG. 10. (a) The hyperbolicity time field $\tau_h(5,\mathbf{x}_0)$. (b) The ellipticity time field $\tau_e(5,\mathbf{x}_0)$.

forward time calculation over the time interval $[5,9]$. Recall that stretching lines are local maximizing lines in the first plot, being the material lines that repel nearby fluid particles for locally the longest time in the flow. Vortex cores filled with elliptic material lines are local maximizing ''patches'' in the second plot. Figure 11 shows the calculation of the field $\sigma(5,\mathbf{x}_0)$ over the same time interval. As we noted earlier, the strongest stretching lines are also local maximizers of this field. Note, however, that weaker stretching lines are suppressed by this approach. Finally, we show the instantaneous local flux plot $\mu(t,5,\mathbf{x}_0)$ for $t=6.5$ and $t=7.5$ in Fig. 12. This technique converges very fast and displays all stretching lines as local minimizing curves with great clarity. Note that there is a local increase in the value of μ before it drops to its minimum, a feature that renders the minimizing curves more visible. A backward time calculation of the same field with $t=4$ and $t=2.5$ is shown in Fig. 13. Again, a very fast convergence to the folding lines (local minimizing curves) leads to great clarity and detail in these plots.

The sharp minimizing nature of stretching and folding lines also results in a loss of detail for longer times, since the thickness of the lines quickly falls below grid resolution. Here we did not address this numerical issue and only calculated the plots for intermediate times. This was possible because of the fast convergence of this approach: in only a few time steps the main hyperbolic LCS emerge and their thickness decreases quickly. This ''thinning'' of hyperbolic LCS is consistent with the predictions of Poje and Haller[13] who proved that the inherent nonuniqueness of finite-time invariant manifolds decreases exponentially as their lifetime increases.

The stretching and folding lines in this simulation have already been approximated in different ways in Poje *et al.*,[23] Haller and Yuan,[25] and Haller.[43] However, none of these methods produced the level of detail and clarity obtained here, and they all needed longer times to converge. It appears that the theoretical framework we developed here captures the essence of these structures.

We finally note that the numerical data set we have studied here does not admit parabolic Lagrangian structures, i.e., shear jets. Our primary goal here was not to explore all possible structures, but illustrate the power of a frame-independent approach on a data set that had been studied previously via other methods. Even in this somewhat simple data set the Eulerian elliptic regions identified from the Okubo–Weiss criterion or potential vorticity plots (cf. Haller and Yuan[25]) differ significantly in size and shape from the actual Lagrangian-elliptic regions we located here. As for the hyperbolic LCS we found here, they remain completely hidden in instantaneous Eulerian calculations (cf. Haller and Yuan[25]).

VIII. CONCLUSIONS

In this paper we have derived a set of frame-independent criteria to locate finite-time hyperbolic, elliptic, and parabolic material lines from general finite-time velocity data. These material lines can in turn be used to identify Lagrangian coherent structures that have a key impact on finite-time advective mixing. We extracted these structures from simulations of two-dimensional turbulence using different ways

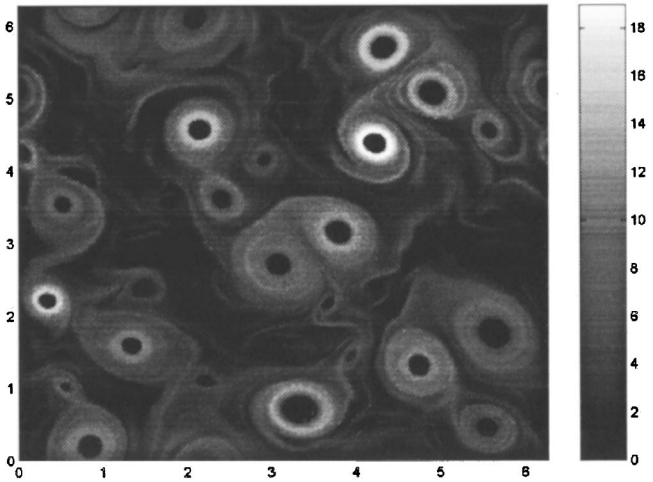

FIG. 11. The scalar field $\sigma(5,\mathbf{x}_0)$.

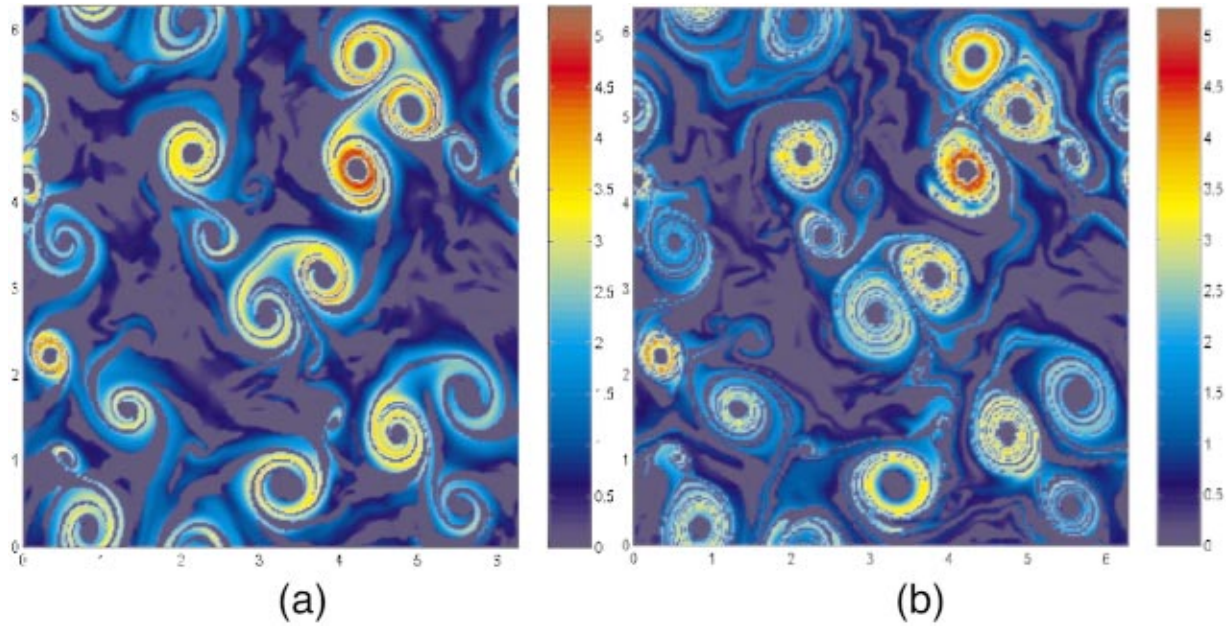

FIG. 12. (Color) The local flux field $\mu(t,5,\mathbf{x}_0)$ for (a) $t=6.5$; (b) $t=7.5$.

of implementing our theorems. Other implementations of our results are clearly possible and may lead to numerical improvements.

In comparison with the earlier analysis of the velocity field in Haller and Yuan,[25] the stretching and folding lines located via the techniques of the current paper are more coherent and better resolved, and the vortex cores are now better identified and understood. In fact, out of all the diagnostic tools that have been proposed (cf. the Introduction), the scalar field $\mu(t,\mathbf{x}_0)$ appears to produce the sharpest results in the shortest time on Lagrangian coherent structures in 2-D turbulence. It reveals a stunning set of stretching and folding lines that connect different mesoscale eddies. These structures are markedly different from the lobes and tangles found in chaotic advection, and their dominance suggests that the primary source of complexity in barotropic turbulent mixing is spatial, not temporal.

If one wishes to locate stretching and folding lines from available particle data, the direct Lyapunov exponent technique proposed in Haller[27] may be the most expedient tool to use. While this ''infinitesimal dispersion'' calculation converges somewhat slowly and produces extra ''ghost'' structures of maximal shear, it is fairly easy to implement. At the same time, it is diagnostic in nature and says nothing about

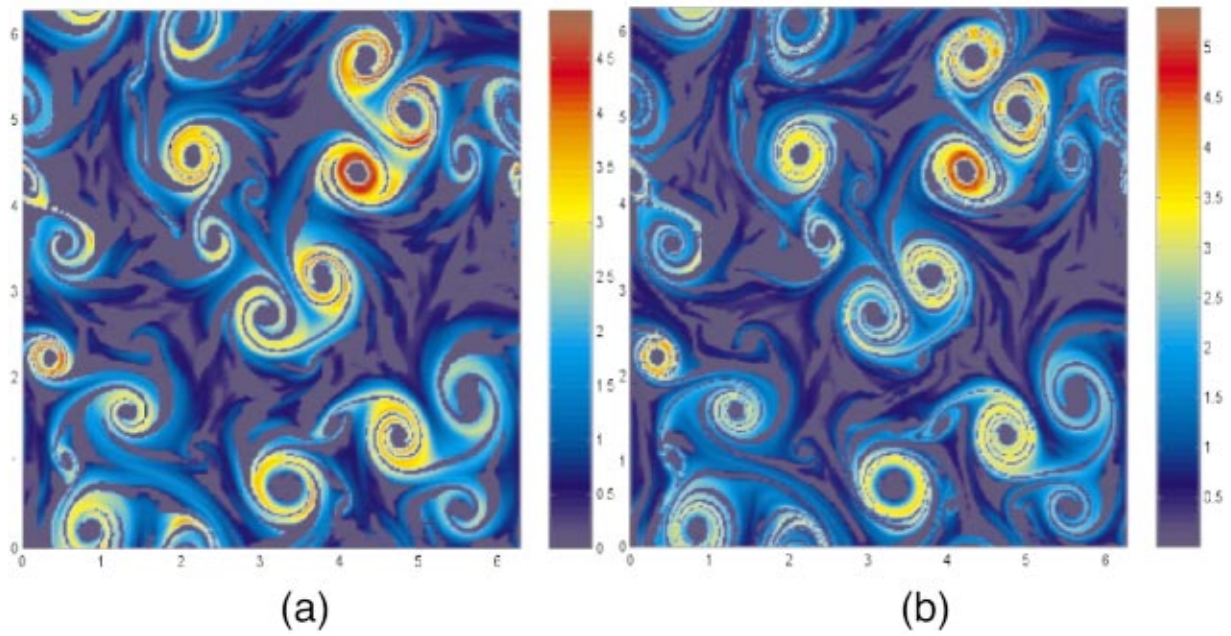

FIG. 13. (Color) The local flux field $\mu(t,5,\mathbf{x}_0)$ for (a) $t=4$; (b) $t=2.5$.

the features of the velocity field that give rise to Lagrangian structures. It is to be contrasted with the dynamic hyperbolicity criterion (16) that gives a direct link between the time history of important Eulerian quantities and Lagrangian mixing. This may ultimately enable one to predict the types of coherent structures that emerge in a particular solution of the Navier–Stokes equation, and the amount of mixing they generate. Knowing the exact Eulerian signatures of intense Lagrangian mixing or lack thereof is also of central importance in a number of applications (see Chaté *et al.*[51]).

Several further questions remain unanswered. One of them is the possible role of the eigenvectors of **M** in Lagrangian mixing. In a recent study Klein *et al.*[48] observed a statistical alignment of tracer gradients with the eigenvectors of a tensor that is simply a scalar multiple of **M**. Making use of the framework we introduced here, one should be able to study this question and find conditions under which the phenomenon occurs. A further question would be how the result we derived here could be extended to three-dimensional turbulence. The 3-D extension of the $\alpha-\beta$ criterion in Haller[43] certainly offers hope that this is possible, although the topological approach we used here needs to be combined with new ideas to extend to higher dimensions. Finding the analog of the dynamic hyperbolicity condition (16) for velocity fields governed by the quasigeostrophic equations would be of great interest in geophysical applications. A more detailed analysis of elliptic coherent structures should also be possible, making more use of the local flux and its two components. Finally, while the types of shear jets we identified here do occur in laminar flows, a more general approach to them is clearly needed. For instance, one could define them as the most ''near-parabolic'' regions in the flow, i.e., regions where one of the eigenvalues of the strain acceleration tensor is close to zero. Such a relaxed definition would certainly be useful in the exploration of geophysical data sets with jets. All these issues are planned for further study and will be reported elsewhere.

ACKNOWLEDGMENTS

The author would like to thank Antonello Provenzale for his permission to use his turbulence solver, and Andrew Poje and Guo-Cheng Yuan for generating the data set analyzed in this paper. He is grateful to one of the anonymous referees for his/her valuable suggestions that have led to several improvements in the manuscript. The author is also indebted to Tieh-Yong Koh and Bernard Legras, who pointed out an error in an earlier formulation of Theorems 2 and 3. Finally, he is thankful to Andrew Poje for a close reading of this paper. This research was partially supported by AFOSR Grant No. F49620-00-1-0133, National Science Foundation Grant No. DMS-98-00922, and a United Technologies research grant.

APPENDIX

1. Proof of Proposition 2

To prove statement (i), we start by introducing a local coordinate **r** defined as $\mathbf{x}=\mathbf{x}_0+\mathbf{r}$. In terms of this new coordinate, the expression (11) for the local flux can be rewritten as

$$\begin{aligned}\varphi(\mathbf{x}_0,t)&=\lim_{\epsilon\to 0}\frac{1}{2\epsilon^2}\int_{\mathcal{S}_\epsilon(0)}|(\mathbf{v}(\mathbf{x}_0+\mathbf{r},t)-\mathbf{v}(\mathbf{x}_0,t))\cdot\mathbf{n}|ds\\&=\lim_{\epsilon\to 0}\frac{1}{2\epsilon^2}\int_{\mathcal{S}_\epsilon(0)}|[\nabla\mathbf{v}(\mathbf{x}_0,t)\mathbf{r}+\mathcal{O}(|\boldsymbol{\xi}|^2)]\cdot\mathbf{n}|ds\\&=\lim_{\epsilon\to 0}\frac{1}{2\epsilon^2}\left\{\int_{\mathcal{S}_\epsilon(0)}|\nabla\mathbf{v}(\mathbf{x}_0,t)\mathbf{r}\cdot\mathbf{n}|\,ds\right.\\&\quad\left.+\int_{\mathcal{S}_\epsilon(0)}|\mathcal{O}(|\mathbf{r}|^2)\cdot\mathbf{n}|ds\right\}.\end{aligned}\tag{A1}$$

Since

$$\lim_{\epsilon\to 0}\frac{1}{2\epsilon^2}\int_{\mathcal{S}_\epsilon(0)}|\mathcal{O}(|\mathbf{r}|^2)\cdot\mathbf{n}|ds\leqslant\lim_{\epsilon\to 0}\frac{1}{\epsilon^2}C\epsilon^2\epsilon\pi=0,$$

the limit of the second integrand in (29) is zero. Letting $\mathbf{r}=\epsilon\boldsymbol{\xi}$, we can therefore rewrite (A1) as

$$\varphi(\mathbf{x}_0,t)=\frac{1}{2}\int_{\mathcal{C}}|\nabla\mathbf{v}(\mathbf{x}_0,t)\boldsymbol{\xi}\cdot\mathbf{n}|ds,$$

with the integral taken over the unit circle $\mathcal{C}$ introduced in Sec. III A.

To evaluate the above integral, recall that the velocity field points inwards on $\mathcal{C}$ within the time-dependent sector $\Psi^-(t)$ and outwards in the sector $\Psi^+(t)$. Since the total flux of the incompressible velocity field is zero over the circle $\mathcal{C}$, we can write

$$\varphi(\mathbf{x}_0,t)=\int_{\mathcal{C}^-(t)}\nabla\mathbf{v}(\mathbf{x}_0,t)\boldsymbol{\xi}\cdot\mathbf{n}ds,\tag{A2}$$

where $\mathcal{C}^-(t)$ denotes the boundary of $\Psi^-(t)$ that falls on the circle $\mathcal{C}$. While this region rotates in time, its area is constant and equals $\pi/2$. Let Z^+ denote the part of Z that bounds $\Psi^-(t)$ along $\boldsymbol{\xi}^+$, and let Z^- denote the part of Z that bounds $\Psi^-(t)$ along $\boldsymbol{\xi}^-$. Applying the Green's theorem to $\Psi^-(t)$ and using incompressibility, we obtain that

$$\begin{aligned}\int_{\mathcal{C}^-(t)}\nabla\mathbf{v}(\mathbf{x}_0,t)\boldsymbol{\xi}\cdot\mathbf{n}ds&=-\int_{Z^+(t)}\nabla\mathbf{v}(\mathbf{x}_0,t)\boldsymbol{\xi}\cdot\mathbf{n}dr\\&\quad-\int_{Z^-(t)}\nabla\mathbf{v}(\mathbf{x}_0,t)\boldsymbol{\xi}\cdot\mathbf{n}dr,\end{aligned}\tag{A3}$$

where **n** denotes the unit normal pointing into $\Psi^-(t)$ in all these integrals, and r is a radial coordinate. Now along $Z^+(t)$ we let $\boldsymbol{\xi}=r\mathbf{e}^+(t)$ (with $|\mathbf{e}^+|=1$), which leads to

$$\begin{aligned}-\int_{Z^+(t)}\nabla\mathbf{v}(\mathbf{x}_0,t)\boldsymbol{\xi}\cdot\mathbf{n}dr&=-2\int_0^1 r\nabla\mathbf{v}(\mathbf{x}_0,t)\mathbf{e}^+\cdot\mathbf{e}^-dr\\&=-\langle\nabla\mathbf{v}\mathbf{e}^+,\mathbf{e}^-\rangle.\end{aligned}$$

A similar calculation gives

$$-\int_{Z^-(t)}\nabla\mathbf{v}(\mathbf{x}_0,t)\boldsymbol{\xi}\cdot\mathbf{n}dr=-\langle\nabla\mathbf{v}\mathbf{e}^-,\mathbf{e}^+\rangle,$$

which, when combined with (A2) and (A3), gives

$$\varphi = -[\langle \nabla \mathbf{v}\mathbf{e}^+, \mathbf{e}^- \rangle + \langle \nabla \mathbf{v}\mathbf{e}^-, \mathbf{e}^+ \rangle]$$
$$= -2\langle \mathbf{S}\mathbf{e}^+, \mathbf{e}^- \rangle = -2\left\langle \mathbf{S}\frac{(\mathbf{e}^+ + \mathbf{e}^-)}{\sqrt{2}}, \frac{(\mathbf{e}^+ + \mathbf{e}^-)}{\sqrt{2}} \right\rangle$$
$$= \sqrt{2}|\mathbf{S}|.$$

Here we used the facts that $(\mathbf{e}^+ + \mathbf{e}^-)/\sqrt{2}$ is precisely the compressional eigenvector of **S,** and the norm of the compressional eigenvalue is just the square root of $|\mathbf{S}|/2$. This completes the proof of statement (i).

To prove statement (ii), we first recall that $\Psi^-(t)$ has constant area. As a result, the instantaneous net flux of the linearized velocity field $\nabla \mathbf{v}(\mathbf{x}_0, t)\boldsymbol{\xi}$ into it is zero.[52] This implies that $\pi\varphi(\mathbf{x}_0, t)$ is equal to the outward flux through the lines Z^+ and Z^-. If $\varphi^\pm(t)$ denotes the flux in the linearized velocity field (6) out of B through $Z^\pm$, then (A2) gives

$$\varphi(\mathbf{x}_0, t) = \varphi^+(t) + \varphi^-(t). \tag{A4}$$

It is this last equation that we shall use below to evaluate the local flux.

The instantaneous net flux of the linearized velocity field through Z^+ can be written as

$$\varphi^+(t) = \int_{Z^+} \left(\dot{\boldsymbol{\xi}} - r\frac{d}{dt}(\mathbf{e}^+) \right) \cdot d\mathbf{n},$$

where the integrand is just the inner product of the relative velocity of the fluid through Z^+ and the unit outward normal $\mathbf{n}$ to Z^+ at the point $\boldsymbol{\xi} = r\mathbf{e}^+(t)$ (with $|\mathbf{e}^+| = 1$). Noting that $\mathbf{n}$ points in the direction of $\nabla\langle \boldsymbol{\xi}, \mathbf{S}\boldsymbol{\xi} \rangle|_{\xi^+}$, we can rewrite the above integral as

$$\varphi^+(t) = 2\int_0^1 \left(\dot{\boldsymbol{\xi}} - r\frac{d}{dt}(\mathbf{e}^+(t)) \right) \cdot \frac{\mathbf{S}\boldsymbol{\xi}^+}{|\mathbf{S}\boldsymbol{\xi}^+|} dr.$$

Differentiating formula (2) in time and using the fact that $\dot{\boldsymbol{\xi}}|_{\xi^+} = \mathbf{A}\boldsymbol{\xi}^+ = r\mathbf{A}\mathbf{e}^+$, we can further rewrite this last expression in the form

$$\varphi^+(t) = \int_0^1 \frac{r}{|\mathbf{S}\mathbf{e}^+|}[\langle 2\mathbf{S}\mathbf{A}\mathbf{e}^+, \mathbf{e}^+ \rangle + \langle \mathbf{e}^+, \dot{\mathbf{S}}\mathbf{e}^+ \rangle] dr$$
$$= \int_0^1 \frac{r}{|\mathbf{S}\mathbf{e}^+|}\langle \mathbf{M}\mathbf{e}^+, \mathbf{e}^+ \rangle dr$$
$$= \frac{1}{2}\frac{\langle \mathbf{e}^+, \mathbf{M}\mathbf{e}^+ \rangle}{|\mathbf{S}\mathbf{e}^+|} = \frac{1}{2}\frac{\langle \boldsymbol{\xi}^+, \mathbf{M}\boldsymbol{\xi}^+ \rangle}{|\boldsymbol{\xi}^+||\mathbf{S}\boldsymbol{\xi}^+|}. \tag{A5}$$

An identical argument establishes the result

$$\varphi^-(t) = \int_{Z^-} \left(\dot{\boldsymbol{\xi}} - r\frac{d}{dt}(\mathbf{e}^-) \right) \cdot d\mathbf{n} = \frac{1}{2}\frac{\langle \boldsymbol{\xi}^-, \mathbf{M}\boldsymbol{\xi}^- \rangle}{|\boldsymbol{\xi}^-||\mathbf{S}\boldsymbol{\xi}^-|}. \tag{A6}$$

By (A4)–(A6), we have

$$\varphi(\mathbf{x}_0, t) = \frac{1}{2}\left(\frac{\langle \boldsymbol{\xi}^+, \mathbf{M}\boldsymbol{\xi}^+ \rangle}{|\boldsymbol{\xi}^+||\mathbf{S}\boldsymbol{\xi}^+|} + \frac{\langle \boldsymbol{\xi}^-, \mathbf{M}\boldsymbol{\xi}^- \rangle}{|\boldsymbol{\xi}^-||\mathbf{S}\boldsymbol{\xi}^-|} \right),$$

as claimed in statement (ii) of Proposition 2.

2. Proof of frame independence for the EPH partition, φ, and $\varphi^\pm$

Let us first assume that $\mathbf{S}(\mathbf{x}, t) \neq \mathbf{0}$. Note that by (1) and (5a), we have

$$\frac{d}{dt}|\boldsymbol{\xi}|_{\xi=\xi^\pm} = 0, \quad \langle \boldsymbol{\xi}^\pm, \mathbf{M}\boldsymbol{\xi}^\pm \rangle = \frac{1}{2}\frac{d^2}{dt^2}|\boldsymbol{\xi}|^2_{\xi=\xi^\pm}.$$

The first equation shows that the orientation of $\boldsymbol{\xi}^\pm$ is frame-independent since it is the zero set of the frame-independent function $(d/dt)|\boldsymbol{\xi}|$.[53] This fact combined with the second equation shows that the sign of $\langle \boldsymbol{\xi}^\pm, \mathbf{M}\boldsymbol{\xi}^\pm \rangle$ is also independent of the frame, since it is given by the sign of $(d^2/dt^2)|\boldsymbol{\xi}|^2$, a frame-independent quadratic form, along the directions $\boldsymbol{\xi}^\pm$. But then (12) implies that the signs of $\varphi^+(\mathbf{x}, t)$ and $\varphi^-(\mathbf{x}, t)$ are frame independent.

Assume now that $\mathbf{S}(\mathbf{x}, t) = \mathbf{0}$, i.e., the point $\mathbf{x}$ belongs to the set $\mathcal{E}(t)$. Performing the change of frame (13), one obtains that in the new frame the gradient of the transformed velocity $\mathbf{u}(\mathbf{y}, t)$ is of the form

$$\nabla \mathbf{u} = \mathbf{Q}^T \nabla \mathbf{v}\mathbf{Q} - \mathbf{Q}^T\dot{\mathbf{Q}}.$$

Since $\mathbf{Q}$ is proper orthogonal, $\mathbf{Q}^T\dot{\mathbf{Q}}$ is skew-symmetric, as one verifies by direct calculation. As a result, at the point $\mathbf{x}$ at time t we have

$$\frac{1}{2}(\nabla \mathbf{u} + \nabla \mathbf{u}^T) = \mathbf{Q}^T\mathbf{S}\mathbf{Q} = \mathbf{0},$$

i.e., the rate of strain also vanishes in the new frame. Consequently, the point $\mathbf{x}$ will belong to the elliptic region $\mathcal{E}(t)$ even after the change of coordinates (13). This completes the argument from the frame independence of the EPH partition.

As for the frame independence of $\varphi^+(\mathbf{x}, t)$ and $\varphi^-(\mathbf{x}, t)$, note that their value only depends on the orientation and not on the magnitude of $\boldsymbol{\xi}^\pm$, as one sees from the formula (12). Then the argument we gave above implies that frame independence of $\varphi^\pm$ and hence that of φ.

3. Proof of Theorem 1

We give a proof that combines a Lyapunov function-type argument with a topological technique, the Wasewsky principle, and with the finite-time invariant manifold results developed in Haller[24] and Haller and Yuan.[25]

Let us consider a trajectory $\mathbf{x}(t)$ generated by the velocity field $\mathbf{v}(\mathbf{x}, t)$, and the associated linearized system,

$$\dot{\boldsymbol{\xi}} = \mathbf{A}(t)\boldsymbol{\xi}, \tag{A7}$$

where $\mathbf{A}(t) = \nabla \mathbf{v}(\mathbf{x}(t), t)$, and the vector $\boldsymbol{\xi}$ is taken from the two-dimensional space $\mathbb{X} = \mathbb{R}^2$. The extended phase space of the $(\boldsymbol{\xi}, t)$ variables will be denoted by $\mathbb{X} \times \mathbb{R}$. By assumption the trajectory $\mathbf{x}(t)$ stays in the hyperbolic region $\mathcal{H}(I)$. As a consequence, the strain acceleration tensor $\mathbf{M}_Z$ is positive definite and the rate-of-strain tensor $\mathbf{S}$ is nondegenerate for all $t \in I$.

We now restrict the linear velocity field (A7) to I, then extend it smoothly to the whole time axis $\mathbb{R}$ in a way that $\mathbf{A}(t)$ [and hence $\mathbf{S}(t)$ and $\mathbf{M}(t)$] become constant matrices outside a slightly larger interval,

$$I^{\epsilon}=[t_0-\epsilon,t_0+\epsilon], \tag{A8}$$

for some small constant $\epsilon>0$. This can be done in a fashion that the function

$$\nu(t)=\min_{\substack{|\mathbf{e}(t)|=1,\\ \mathbf{e}(t)\in Z}}\langle \mathbf{e}(t),\mathbf{M}(t)\mathbf{e}(t)\rangle>0, \tag{A9}$$

and $\lambda(t)$, the negative eigenvalue of $\mathbf{S}(t)$, satisfy

$$\begin{aligned}&\nu(t)\geqslant \nu_{\min}\overset{\text{def.}}{=}\min_{t\in I}\nu(t)-\epsilon,\\ &\lambda(t)\geqslant \lambda_{\min}\overset{\text{def.}}{=}\min_{t\in I}\lambda(t)-\epsilon,\ t\in\mathbb{R}.\end{aligned} \tag{A10}$$

(For the details of this construction, see Haller.)[24] We select $\epsilon>0$ small enough so that

$$\nu_{\min}>0,\ \lambda_{\min}<0.$$

We also note that by the continuity of $\langle \mathbf{e},\mathbf{Me}\rangle$ in $\mathbf{e}$, for all small enough $\epsilon>0$, we have

$$\min_{\substack{|\mathbf{e}(t)|=1,\\ \text{dist}\,(\mathbf{e}(t),Z)<\epsilon}}\langle \mathbf{e}(t),\mathbf{M}(t)\mathbf{e}(t)\rangle>\frac{\nu_{\min}}{2}. \tag{A11}$$

We will now establish several properties of the smoothly extended linear system. For simplicity, we keep the same notation for the extended system, i.e., keep referring to (A7) when we discuss the properties of its infinite-time extension.

(a) $\boldsymbol{\xi}=\mathbf{0}$ has a stable manifold E^s. Since the rate-of-strain matrix $\mathbf{S}$ is indefinite, the quadratic form $C(\boldsymbol{\xi},t)=\langle \boldsymbol{\xi},\mathbf{S}\boldsymbol{\xi}\rangle$ takes both positive and negative values in any open neighborhood of the origin $\boldsymbol{\xi}=\mathbf{0}$. Also by assumption, the derivative of C along solutions,

$$\begin{aligned}\dot{C}(\boldsymbol{\xi},t)&=\langle \dot{\boldsymbol{\xi}},\mathbf{S}\boldsymbol{\xi}\rangle+\langle \boldsymbol{\xi},\mathbf{S}\dot{\boldsymbol{\xi}}\rangle+\langle \boldsymbol{\xi},\dot{\mathbf{S}}\boldsymbol{\xi}\rangle\\ &=\langle \mathbf{SA}\boldsymbol{\xi},\boldsymbol{\xi}\rangle+\langle \boldsymbol{\xi},\mathbf{SA}\boldsymbol{\xi}\rangle+\langle \boldsymbol{\xi},\dot{\mathbf{S}}\boldsymbol{\xi}\rangle=\langle \boldsymbol{\xi},\mathbf{M}\boldsymbol{\xi}\rangle,\end{aligned} \tag{A12}$$

is positive definite for all $\boldsymbol{\xi}\in Z$, and $t\in I$ [and hence for all $t\in\mathbb{R}$ by (A10)]. It then follows from (A12) that

$$\dot{C}(\boldsymbol{\xi},t)\geqslant \nu_{\min}|\boldsymbol{\xi}|^2,\ \boldsymbol{\xi}\in Z,\ t\in\mathbb{R}. \tag{A13}$$

Next, we want to argue that the extended system (A7) admits a solution that converges to the origin. Since C is indefinite, there exists a region Ψ^- in the extended phase space such that

$$\Psi^-=\{(\xi,t)\in\mathbb{X}\times\mathbb{R}\,\|\boldsymbol{\xi}|\leqslant 1,\quad C(\boldsymbol{\xi},t)\leqslant 0\}. \tag{A14}$$

We denote the boundary of Ψ^- by $\partial\Psi^-$, and the interior of Ψ^- by $i(\Psi^-)=\Psi^--\partial\Psi^-$. [We also recall that the $t=$const slice of Ψ^- is denoted by $\Psi^-(t)$, with its boundary denoted by $\partial\Psi^-(t)$.] Let us consider a trajectory $\boldsymbol{\xi}(t)$ which satisfies $\boldsymbol{\xi}(t_0)=\boldsymbol{\xi}_0\in\Psi(t_0)$. Observe that as long as $\boldsymbol{\xi}(t)\in i(\Psi^-(t))$, its norm $|\boldsymbol{\xi}(t)|$ decreases monotonically by the estimate

$$\frac{d}{dt}|\boldsymbol{\xi}|^2=\frac{d}{dt}\langle \boldsymbol{\xi},\boldsymbol{\xi}\rangle=2\langle \dot{\boldsymbol{\xi}},\boldsymbol{\xi}\rangle=2\langle \boldsymbol{\xi},\mathbf{S}\boldsymbol{\xi}\rangle=2C(\boldsymbol{\xi},t)<0, \tag{A15}$$

where we used (A14) from above. We claim that if $\boldsymbol{\xi}(t)\in i(\Psi^-(t))$ for all $t\geqslant t_0$, then $\boldsymbol{\xi}(t)$ tends to the origin as $t\to\infty$.

Assume the contrary, in which case, by (A15), there exists a positive number $\delta\leqslant|\boldsymbol{\xi}(t_0)|$ such that

$$|\boldsymbol{\xi}(t)|>\delta,\ t>t_0. \tag{A16}$$

Consider then an unbounded, monotone sequence of times $\{t_k\}_{k=0}^{\infty}$. By (A15), $|\boldsymbol{\xi}(t_k)|$ is a bounded, monotone sequence and hence it converges to some $\sigma>0$. By the continuity of $\boldsymbol{\xi}(t)$, this implies

$$\lim_{t\to\infty}|\boldsymbol{\xi}(t)|=\sigma. \tag{A17}$$

By the monotonicity of $|\boldsymbol{\xi}(t)|$, we must then have $\lim_{t\to\infty}|\dot{\boldsymbol{\xi}}(t)|=0$, which together with (A16), (A17), and (A15) implies that

$$\lim_{t\to\infty}\text{dist}\,(\boldsymbol{\xi}(t),Z)=0. \tag{A18}$$

Then selecting $\epsilon>0$ small enough in (A11), formulas (A18) and (A11) imply

$$\langle \boldsymbol{\xi}(t),\mathbf{M}(t)\boldsymbol{\xi}(t)\rangle>\frac{\nu_{\min}}{2}|\boldsymbol{\xi}(t)|^2,\quad t>T^*, \tag{A19}$$

for some finite $T^*>t_0$. Using (A16) and (A19), we can then write

$$\begin{aligned}0>C(\boldsymbol{\xi}(t),t)&=C(\boldsymbol{\xi}_0,t_0)+\int_{t_0}^{T^*}\dot{C}(\boldsymbol{\xi}(\tau),\tau)d\tau\\ &\quad+\int_{T^*}^{t}\dot{C}(\boldsymbol{\xi}(\tau),\tau)d\tau\geqslant C(\boldsymbol{\xi}_0,t_0)\\ &\quad+\int_{t_0}^{T^*}\dot{C}(\boldsymbol{\xi}(\tau),\tau)\,d\tau+\frac{\nu_{\min}}{2}\delta^2(t-T^*),\end{aligned} \tag{A20}$$

for all $t>T^*$, which is a contradiction for t large enough, since the first two terms on the right-hand-side of this inequality are bounded. Therefore, we indeed have

$$\boldsymbol{\xi}(t)\in i(\Psi^-(t)),\ t\geqslant t_0\Rightarrow\lim_{t\to\infty}\boldsymbol{\xi}(t)=\mathbf{0}. \tag{A21}$$

Now we want to argue that there are solutions of the extended system (A7) that actually stay in $i(\Psi^-(t))$ for all $t\geqslant t_0$. Showing the instantaneous linear flow geometry in the strain eigenbasis $\{\hat{\boldsymbol{\xi}}_1,\hat{\boldsymbol{\xi}}_2\}$. Figure 14 helps in verifying some general properties of $\partial\Psi^-$.

(α) On the boundary component $V^1=\partial\Psi^-\cap\{|\boldsymbol{\xi}|=1\}$ the vector field points inwards by (A15).

(β) On the boundary component $V^2=\partial\Psi^-\cap Z-\{\boldsymbol{\xi}=\mathbf{0}\}$ the extended vector field (A7) points strictly outwards. This follows by observing that on V^2 we have $C\equiv 0$, while on any nontrivial trajectory we have $\dot{C}>0$, by (A13).

(γ) The boundary component $V^3=\partial\Psi^--V^1-V^2$ is just the invariant line $\{\boldsymbol{\xi}=\mathbf{0}\}$.

(δ) As a consequence of (α)–(γ), the set of points immediately leaving Ψ^- is given by $W^{im}=V^2$.

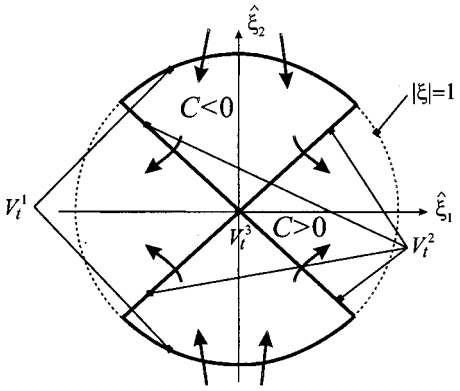

FIG. 14. Instantaneous flow geometry and the set $\partial\Psi^-(t)$ under the assumption that the matrix $\mathbf{M}(t)$ is positive definite. The coordinates $\hat{\xi}_i$ are defined relative to the eigenbasis of $\mathbf{S}$.

(ε) Let us denote the set of points eventually leaving Ψ^- by W^{ev}. By definition, $W^{im}\subset W^{ev}$. Since V^3 is clearly not contained in W^{ev}, we conclude that W^{im} is relatively closed in W^{ev}.[54]

(φ) Ψ^- is a closed set.

By definition, the properties (δ)–(φ) make Ψ^- a Wasewsky set (see, e.g., Hale[41]). As a consequence, the following result (the Wasewsky principle) holds for Ψ^-: The map

$$\Gamma: W^{ev}\to W^{im} \tag{A22}$$

that maps initial conditions in W^{ev} to the point where they leave Ψ^-, is continuous.

We now use the Wasewsky principle to argue that there are nontrivial solutions that stay in Ψ^- for all times. Suppose the contrary, i.e., suppose that all nonzero solutions leave Ψ^- eventually. As a result, $W^{ev}=\Psi^- - V^3$ and hence $\Gamma(\Psi^- - V^3)=V^2$. But a continuous map cannot map the connected set $\Psi^- - V^3$ onto the disconnected set V^2, thus we have established a contradiction. We can therefore conclude that there exists a solution $\boldsymbol{\xi}^*(t)$ that stays in Ψ^- for all times. By (A21), $\boldsymbol{\xi}^*(t)$ must necessarily converge to zero, i.e., the $\boldsymbol{\xi}=\mathbf{0}$ solution of the extended system (A7) has a stable manifold, which we denote by E^s.[55]

For later use, we now estimate the rate at which solutions in E^s converge to the trivial solution. Let E^s_t denote the $t=$const section of E^s_t, and let $\mathbf{e}(t)$ be a unit vector in E^s_t. Note that $\mathbf{e}(t)$ can be chosen as a continuous function of t. For that reason the function $\langle \mathbf{e}(t),\mathbf{S}(t)\mathbf{e}(t)\rangle$ is continuous in t and hence admits a maximum over the compact interval I. Since E^s lies in the interior of the sector Ψ^-, this maximum is less than zero. Selecting $\epsilon>0$ small enough in the definition of I^ϵ [cf. (A8)], we can therefore ensure that

$$a \overset{\text{def.}}{=} -\max_{t\in I^\epsilon}\langle \mathbf{e}(t),\mathbf{S}(t)\mathbf{e}(t)\rangle = -\max_{t\in\mathbb{R}}\langle \mathbf{e}(t),\mathbf{S}(t)\mathbf{e}(t)\rangle > 0.$$

Combining the definition of a with the inequality (A15), we obtain that for any $\boldsymbol{\xi}(t)\in E^s_t$,

$$\begin{aligned}\frac{d}{dt}|\boldsymbol{\xi}|^2 &= 2\langle \boldsymbol{\xi},\mathbf{S}\boldsymbol{\xi}\rangle = 2|\boldsymbol{\xi}|^2\langle \mathbf{e}(t),\mathbf{S}(t)\mathbf{e}(t)\rangle \\ &\le 2|\boldsymbol{\xi}|^2\max_{t\in\mathbb{R}}\langle \mathbf{e}(t),\mathbf{S}(t)\mathbf{e}(t)\rangle \\ &\le -2a|\boldsymbol{\xi}|^2.\end{aligned}$$

Integrating this inequality yields

$$|\boldsymbol{\xi}(t)|\le|\boldsymbol{\xi}(t_0)|e^{-a(t-t_0)}, \tag{A23}$$

for all solutions with $\boldsymbol{\xi}(t_0)\in E^s_{t_0}$.

(b) $\boldsymbol{\xi}=\mathbf{0}$ has an unstable manifold E^u. This follows by repeating the argument given in (a) in backward time over the interval I_u. That is possible since reversing time in the extended equation (A7) gives

$$\dot{\boldsymbol{\xi}}=-\mathbf{A}(-t)\boldsymbol{\xi},$$

and hence the strain matrix $\hat{\mathbf{S}}(t)=-\frac{1}{2}(\mathbf{A}(-t)-\mathbf{A}(-t))=-\mathbf{S}(-t)$ remains indefinite and $\hat{\mathbf{M}}(t)=\mathbf{M}(-t)$ remains positive definite on Z. As a result, we can conclude the existence of an unstable manifold $E^u\subset\mathbb{X}\times\mathbb{R}$ for the trivial solution of the extended system (A7). In analogy with (A23), solutions in E^u obey a growth estimate,

$$|\boldsymbol{\xi}(t)|\ge|\boldsymbol{\xi}(t_0)|e^{a(t-t_0)}.$$

The exponent a in this estimate is the same as in (A23), which follows from incompressibility and Liouville's theorem. [Since $\mathrm{tr}(\mathbf{A})=0$, the determinant of any fundamental matrix of (A7) is constant in time.]

(c) The dimension of E^s and E^u. The dimension of E^s and E^u can be found by invoking the continuity of the Wasewsky map Γ defined in (A22). In particular, consider Fig. 14 and note that for Γ to be continuous, $V^1_t\cap W^{ev}$ must be a union of two open sets, separated by $E^s_t\cap\{|\boldsymbol{\xi}|=1\}$. Since this latter set is a point, by the continuity of Γ we conclude that $\dim E^s_t=1$, which implies that $\dim E^s=2$ in the extended phase space $\mathbb{X}\times\mathbb{R}$. Since the dimensions of E^s_t and E^u_t add up to the dimension of $\mathbb{X}$, we obtain that $\dim E^u=2$.

(d) $\mathbf{x}(t)$ is contained in a repelling material line. Since E^s_t and E^u_t are lines, we can "flatten" out the invariant manifolds E^s and E^u by introducing a linear change of coordinates,

$$\boldsymbol{\xi}=\mathbf{R}(t)\,\boldsymbol{\eta}. \tag{A24}$$

For any t, the columns of $\mathbf{R}(t)$ are chosen to be a linearly independent set of unit vectors taken from $E^s_t\cup E^u_t$. In the $\boldsymbol{\eta}$ coordinates the extended system (A7) takes the form

$$\dot{\boldsymbol{\eta}}=\begin{pmatrix} q^s(t) & 0\\ 0 & q^u(t)\end{pmatrix}\boldsymbol{\eta}, \tag{A25}$$

with two scalar functions $q^s(t)$ and $q^u(t)=-q^s(t)$. We partition $\boldsymbol{\eta}$ accordingly into $\boldsymbol{\eta}=(\eta^s,\eta^u)$. The solution components can be written as

$$\eta^s(t)=\Phi^s(t)\,\eta^s(t_0),\quad \eta^u(t)=\Phi^u(t)\,\eta^u(t_0),$$

with the estimates

$$\|\Phi^s(t)\|\le e^{-a(t-t_0)},\quad \|\Phi^u(t)\|\ge e^{a(t-t_0)}, \tag{A26}$$

for all $t\in I$.

Now let us return to the underlying trajectory $\mathbf{x}(t)$ and let $\boldsymbol{\xi}=\mathbf{x}-\mathbf{x}(t)$ denote a new local coordinate along the trajectory. Differentiating this change of variables with respect to t, Taylor expanding $\mathbf{v}(\mathbf{x}(t)+\boldsymbol{\xi},t)$ in $\boldsymbol{\xi}$, and then switching to the variable $\boldsymbol{\eta}$ introduced in (A25), we obtain the differential equation

$$\dot{\boldsymbol{\eta}}=\begin{pmatrix} q^s(t) & 0 \\ 0 & q^u(t) \end{pmatrix}\boldsymbol{\eta}+\mathbf{f}(\boldsymbol{\eta},t),$$

where, for any fixed $t\in I$ we have $\mathbf{f}(\boldsymbol{\eta},t)=\mathcal{O}(|\boldsymbol{\eta}|^2)$. For equations of this form satisfying decay estimates of the type (A26), we showed in Haller[24] the existence of smooth finite-time stable and unstable manifolds $W^s(\mathbf{0})$ and $W^u(\mathbf{0})$ in the extended phase.[56] Here $\dim W^s(\mathbf{0})=\dim E^s=2$ and $\dim W^u(\mathbf{0})=\dim E^u=2$, and the manifolds are tangent to E^s and E^u, respectively, along the solution $\boldsymbol{\eta}\equiv\mathbf{0}$, i.e., along the trajectory $\mathbf{x}(t)$ for $t\in I$. [These invariant manifolds are not unique, but the distance of, say, two unstable manifolds is of the order $\mathcal{O}(e^{-K(t_2-t_1)})$, i.e., decays exponentially as the length of the interval I increases.] We can, therefore, conclude that $\mathbf{x}(t)$ is contained in a repelling material line (finite-time stable manifold). We note that $\mathbf{x}(t)$ is also contained in an attracting material line (finite-time unstable manifold).

4. Proof of Theorem 2

Statement (i) follows from an inspection of the solutions of (6) in the case $\mathbf{x}(t)\in\mathcal{P}(J)$, where J is any subinterval within I. Indeed, no material lines formed by the solutions given in (10) are finite-time hyperbolic. Therefore, hyperbolic material lines cannot spend a whole interval of time J in the parabolic region.

The proof of statement (ii) will follow immediately from the proof of Theorem 3 given below. In particular, see formula (A28).

5. Proof of Theorem 3

Since the trajectory $\mathbf{x}(t)$ is assumed to stay in the elliptic region $\mathcal{E}(I)$, $\mathbf{M}_Z$ is indefinite for all $t\in I$. As a result, on precisely one of the sides of the sector $\psi^-(t)$ the flux is negative, i.e., fluid is flowing into the interior of $\psi^-(t)$. We assume that this happens on the side spanned by Z^-, if not, we simply change the indices of $\boldsymbol{\xi}^+$ and $\boldsymbol{\xi}^-$ in our notation.

Assume the contrary of the statement of the theorem, i.e., assume that the trajectory $\mathbf{x}(t)$ is finite-time hyperbolic. By definition, this implies that the $\boldsymbol{\xi}=\mathbf{0}$ solution of the linearized equation (6) is finite-time hyperbolic. In that case it must admit finite-time stable and unstable manifolds over the interval I. These manifolds are actually vector bundles (i.e., their $t=$const sections are lines) by the linearity of (6). E^s_t, the $t=$const section of a finite-time stable manifold of the origin, must lie in the interior of the time-dependent sector $\Psi^-(t)$ where the distance of trajectories from the origin strictly decreases.

Consider the time-dependent sector $\mathcal{T}(t)$ enclosed by E^s_t, the line $Z^-(t)$, and the $\mathcal{C}^s(t)$ arc of the unit circle that connects these lines. Since $E^s_t\subset\Psi^-(t)$, we must have

$$\text{Area}\,(\mathcal{T}(t))<\frac{\pi}{4}, \tag{A27}$$

i.e., the area of the sector $\mathcal{T}(t)$ cannot reach that of $\Psi^-(t)$. Note, however, that the area of $\mathcal{T}(t)$ is increasing since the net flux into it is positive both along the boundary $Z^-(t)$ as well as along $\mathcal{C}^s(t)$, while it is zero along E^s_t by the invariance of the stable manifold E^s. We can therefore write for any $t\in I=[t_1,t_2]$ that

$$\text{Area}\,(\mathcal{T}(t))=\text{Area}\,(\mathcal{T}(t_1))+\int_{t_1}^{t}\int_{\mathcal{C}^s(\tau)}\nabla\mathbf{v}(\mathbf{x}_0,\tau)\boldsymbol{\xi}\cdot\mathbf{n}\;ds\,d\tau+\frac{1}{2}\int_{t_1}^{t}|\varphi_0(\mathbf{x}_0,\tau)|d\tau,$$

where the first integral is the total fluid area entering $\mathcal{T}(t)$ along the boundary $\mathcal{C}^s(t)$, and the second integral is the area entering along $Z^-(t)$. The above equation leads to the estimate

$$\text{Area}\,(\mathcal{T}(t))>\frac{1}{2}\int_{t_1}^{t}|\varphi_-(\mathbf{x}_0,\tau)|d\tau,$$

which, together with (A27), gives the estimate

$$\int_{t_1}^{t_2}|\varphi_0(\mathbf{x}_0,\tau)|d\tau<\frac{\pi}{2}. \tag{A28}$$

But (A28) establishes a contradiction with assumption (14) of the theorem, thus $\mathbf{x}(t)$ cannot be finite-time hyperbolic over the interval I.

6. Proof of Theorem 5

To prove the theorem, we use Eq. (15) to rewrite the strain acceleration tensor in the form

$$\mathbf{M}=\mathbf{S}^2+2\mathbf{S}\boldsymbol{\Omega}-\boldsymbol{\Omega}^2-\frac{1}{\rho}\mathbf{P}+\nu\nabla^2\mathbf{S}+\mathbf{G}. \tag{A29}$$

We recall that at any fixed time t, the hyperbolic region $\mathcal{H}(t)$ is defined as the spatial region satisfying

$$\langle\boldsymbol{\xi}^+,\mathbf{M}\boldsymbol{\xi}^+\rangle>0,\ \langle\boldsymbol{\xi}^-,\mathbf{M}\boldsymbol{\xi}^-\rangle>0. \tag{A30}$$

In what follows we take the zero strain directions $\boldsymbol{\xi}^{\pm}$ to be unit vectors for computational simplicity.

To obtain a sufficient dynamic condition on Lagrangian hyperbolicity, we shall derive a single condition that implies both conditions in (A30). Therefore, if this new single condition is satisfied over a time interval I along a trajectory $\mathbf{x}(t)$, then this trajectory is contained in a hyperbolic material line over I by Theorem 1.

To evaluate the conditions (A30) using the expression (A29) for $\mathbf{M}$, we first note that the directions of zero strain obey the relation

$$\boldsymbol{\xi}^{\pm}=\frac{\mathbf{e}_1\pm\mathbf{e}_2}{\sqrt{2}}, \tag{A31}$$

where $\mathbf{e}_i$ denote the unit eigenvectors of the rate-of-strain with the properties

$$\mathbf{S}\mathbf{e}_1=s\mathbf{e}_1,\quad \mathbf{S}\mathbf{e}_2=-s\mathbf{e}_2,\quad s\geqslant 0.$$

For concreteness, we also fix a particular orientation for $\mathbf{e}_1$ and $\mathbf{e}_2$ by requiring

$$\mathbf{e}_1 \times \mathbf{e}_2 > 0. \tag{A32}$$

Then, using (A31) we obtain the following identities:

$$\begin{aligned}
\langle \boldsymbol{\xi}^{\pm}, \mathbf{S}^2 \boldsymbol{\xi}^{\pm} \rangle &= \frac{s^2}{2} \langle \mathbf{e}_1 \pm \mathbf{e}_2, \mathbf{e}_1 \pm \mathbf{e}_2 \rangle = s^2, \\
\langle \boldsymbol{\xi}^{\pm}, 2\mathbf{S}\boldsymbol{\Omega}\boldsymbol{\xi}^{\pm} \rangle &= -2 \langle \boldsymbol{\xi}^{\pm}, \boldsymbol{\Omega}\mathbf{S}\boldsymbol{\xi}^{\pm} \rangle \\
&= -\langle \mathbf{e}_1 \pm \mathbf{e}_2, \boldsymbol{\Omega}\mathbf{S}(\mathbf{e}_1 \pm \mathbf{e}_2) \rangle \\
&= \mp 2s \langle \boldsymbol{\Omega}\mathbf{e}_1, \mathbf{e}_2 \rangle = \mp s\omega, \\
\langle \boldsymbol{\xi}^{\pm}, -\boldsymbol{\Omega}^2 \boldsymbol{\xi}^{\pm} \rangle &= |\boldsymbol{\Omega}\boldsymbol{\xi}^{\pm}| = \frac{\omega^2}{4}.
\end{aligned}$$

Here, in the second identity, we used the orientation rule (A32) as well as the fact that for two-dimensional incompressible flows, $\mathbf{S}\boldsymbol{\Omega} = -\boldsymbol{\Omega}\mathbf{S}$. Using the three identities above together with (A29), we can rewrite the conditions (A30) as

$$(s \mp \omega/2)^2 - \frac{1}{\rho} \langle \boldsymbol{\xi}^{\pm}, \mathbf{P}\boldsymbol{\xi}^{\pm} \rangle + \nu \langle \boldsymbol{\xi}^{\pm}, \nabla^2 \mathbf{S}\boldsymbol{\xi}^{\pm} \rangle + \langle \boldsymbol{\xi}^{\pm}, \mathbf{G}\boldsymbol{\xi}^{\pm} \rangle > 0.$$

Recalling that $s \geqslant 0$, we find that both of these conditions hold if

$$(s - |\omega|/2)^2 - \frac{1}{\rho} \langle \boldsymbol{\xi}^{\pm}, \mathbf{P}\boldsymbol{\xi}^{\pm} \rangle + \nu \langle \boldsymbol{\xi}^{\pm}, \nabla^2 \mathbf{S}\boldsymbol{\xi}^{\pm} \rangle + \langle \boldsymbol{\xi}^{\pm} \mathbf{G}\boldsymbol{\xi}^{\pm} \rangle > 0. \tag{A33}$$

Using the quantities introduced in Sec. IV C and recalling that $\boldsymbol{\xi}^{\pm}$ are unit vectors, we can write down the following estimates:

$$\langle \boldsymbol{\xi}^{\pm}, \mathbf{P}\boldsymbol{\xi}^{\pm} \rangle \leqslant \kappa, \quad -\langle \boldsymbol{\xi}^{\pm}, \nabla^2 \mathbf{S}\boldsymbol{\xi}^{\pm} \rangle \leqslant \sigma, \quad -\langle \boldsymbol{\xi}^{\pm}, \mathbf{G}\boldsymbol{\xi}^{\pm} \rangle \leqslant \gamma.$$

From these estimates we obtain that (A34) is satisfied if condition of (16) of Theorem 5 holds, which completes the proof.

[1] H. Aref and M. S. El Naschie, *Chaos Applied to Fluid Mixing* (Pergamon, New York, 1995).
[2] V. Rom-Kedar, "Homoclinic tangles-classification and applications," Nonlinearity **7**, 441 (1994).
[3] J. M. Ottino, *The Kinematics of Mixing: Stretching, Chaos, and Transport* (Cambridge University Press, Cambridge, 1989).
[4] N. Malhotra and S. Wiggins, "Geometric structures, lobe dynamics, and Lagrangian transport in flows with a periodic time-dependence, with applications to Rossby wave flow," J. Nonlinear Sci. **8**, 401 (1998).
[5] D. Elhmaïdi, A. Provenzale, and A. Babiano, "Elementary topology of two-dimensional turbulence from a Lagrangian viewpoint and single-particle dispersion," J. Fluid Mech. **257**, 533 (1993).
[6] E. M. Ziemniak, C. Jung, and T. Tél, "Tracer dynamics in open hydrodynamical flows as chaotic scattering," Physica D **44**, 1234 (1994).
[7] H. Ridderinkhof and J. W. Lober, "Lagrangian characterization of circulation over submarine banks with application to the Gulf of Maine," J. Phys. Oceanogr. **24**, 1184 (1994).
[8] P. D. Miller, C. K. R. T. Jones, A. M. Rogerson, and L. J. Pratt, "Quantifying transport in numerically generated velocity fields," Physica D **110**, 105 (1997).
[9] A. M. Rogerson, P. D. Miller, L. J. Pratt, and C. K. R. T. Jones, "Lagrangian motion and fluid exchange in a barotropic meandering jet," J. Phys. Oceanogr. **29**, 2635 (1999).
[10] T.-Y. Koh and R. A. Plumb, "Lobe dynamics applied to barotropic Rossby-wave breaking," Phys. Fluids **12**, 1518 (2000).
[11] C. Coulliette and S. Wiggins, "Intergyre transport in a wind-driven, quasi-geostrophic double gyre: An application of lobe dynamics," Nonlinear Proc. Geophys. **8**, 69 (2001).
[12] G. Haller and A. C. Poje, "Finite-time transport in aperiodic flows," Physica D **119**, 352 (1998).
[13] A. C. Poje and G. Haller, "Geometry of cross-stream mixing in a double-gyre ocean model," J. Phys. Oceanogr. **29**, 1649 (1999).
[14] O. M. Velasco Fuentes, "Chaotic advection by two interacting finite-area vortices," Phys. Fluids **13**, 901 (2001).
[15] K. Bowman, "Manifold geometry and mixing in observed atmospheric flows," preprint, 1999.
[16] C. K. R. T. Jones and S. Winkler, "Do invariant manifolds hold water?" in *Handbook of Dynamical Systems III: Towards Applications*, edited by B. Fiedler, G. Iooss, and N. Kopell (Springer-Verlag, New York, to be published).
[17] S. Winkler, "Lagrangian dynamics in geophysical fluid flows," Ph.D. thesis, Brown University, 2001.
[18] R. T. Pierrehumbert, "Large-scale horizontal mixing in planetary atmospheres," Phys. Fluids A **3**, 1250 (1991).
[19] R. T. Pierrehumbert and H. Yang, "Global chaotic mixing on isentropic surfaces," J. Atmos. Sci. **50**, 2462 (1993).
[20] B. Joseph and B. Legras, "On the relation between kinematic boundaries, stirring, and barriers for the Antarctic polar vortex," J. Atmos. Sci. (in press).
[21] N. Malhotra, I. Mezić, and S. Wiggins, "Patchiness: A new diagnostic for Lagrangian trajectory analysis in time-dependent fluid flows," Int. J. Bifurcation Chaos Appl. Sci. Eng. **8**, 1053 (1998).
[22] I. Meziç and S. Wiggins, "A method for visualization of invariant sets of dynamical systems based on the ergodic partition," Chaos **9**, 213 (1999).
[23] A. C. Poje, G. Haller, and I. Mezić, "The geometry and statistics of mixing in aperiodic flows," Phys. Fluids **11**, 2963 (1999).
[24] G. Haller, "Finding finite-time invariant manifolds in two-dimensional velocity fields," Chaos **10**, 99 (2000).
[25] G. Haller and G. Yuan, "Lagrangian coherent structures and mixing in two-dimensional turbulence," Physica D **147**, 352 (2000).
[26] G. Lapeyre, B. L. Hua, and B. Legras, "Comment on 'Finding finite-time invariant manifolds in two-dimensional velocity fields' [Chaos **10**, 99 (2000)]," Chaos **11**, 427 (2001).
[27] G. Haller, "Distinguished material surfaces and coherent structures in 3D fluid flows," Physica D **149**, 238 (2001).
[28] A. Provenzale, A. Babiano, and A. Zanella, "Dynamics of Lagrangian tracers in barotropic turbulence," in *Mixing: Chaos and Turbulence*, edited by H. Chate, J. M. Chomaz, and E. Villermaux (Plenum, New York, 1999).
[29] If $\mathbf{S}$ is nonzero but its diagonal elements are zero (parallel shear flow), then we can select $\boldsymbol{\xi}^{+} = (1,0)$ and $\boldsymbol{\xi}^{-} = (0,1)$.
[30] The symmetry of the matrix $\mathbf{S}\nabla\mathbf{v}$ follows from incompressibility for two-dimensional flows.
[31] We note that if the velocity field $\mathbf{v}$ is a solution of the Navier–Stokes equation with no body forces, then we have $\dot{\mathbf{S}} = -(\mathbf{S}^2 + \boldsymbol{\Omega}^2) - (1/\rho)\mathbf{P} + \nu\nabla^2\mathbf{S}$, where $\boldsymbol{\Omega}$ is the skew-symmetric part of the velocity gradient, $\mathbf{P}$ denotes the pressure Hessian, and ρ and ν refer to density and kinematic viscosity, respectively (see, e.g., Tabor and Klapper[32]).
[32] M. Tabor and I. Klapper, "Stretching and alignment in chaotic and turbulent flows," in *Chaos Applied to Fluid Mixing*, edited by H. Aref and M. S. El Naschie (Pergamon, New York, 1995).
[33] B. A. Cotter and R. S. Rivlin, "Tensors associated with time-dependent stress," Quarterly Appl. Math. **13**, 177 (1955).
[34] Gy. Béda, I. Kozák, and J. Verhás, *Continuum Mechanics* (Akadémia Kiadó, Budapest, 1995).
[35] By infinitesimal perturbations we mean perturbations advected by the flow linearized along the material line.
[36] This is why resonance-related instabilities are confined to layers of width $\mathcal{O}(\sqrt{\epsilon})$ in $\mathcal{O}(\epsilon)$ time-periodic perturbations of generic steady velocity fields with closed streamlines [cf. V. I. Arnold, *Mathematical Methods of Classical Mechanics* (Springer-Verlag, New York, 1978)].
[37] A. Okubo, "Horizontal dispersion of floatable trajectories in the vicinity of velocity singularities such as convergencies," Deep-Sea Res. **17**, 445 (1970).
[38] J. Weiss, "The dynamics of enstropy transfer in 2-dimensional hydrodynamics," Physica D **48**, 273 (1991).
[39] In particular, $\det(\nabla\mathbf{v}) > 0$ would mean a pair of purely imaginary eigenvalues and $\det(\nabla\mathbf{v}) < 0$ would mean a positive and a negative real eigenvalue for the constant matrix $\nabla\mathbf{v}$.

[40]F. Verhulst, *Nonlinear Differential Equations and Dynamical Systems* (Springer-Verlag, Berlin, 1990).
[41]J. K. Hale, *Ordinary Differential Equations* (Kreiger, New York, 1980).
[42]C. Basdevant and T. Philipovitch, ''On the validity of the 'Weiss criterion' in two-dimensional turbulence,'' Physica D **73**, 17 (1994).
[43]G. Haller, ''Response to 'Comment on ''Finding finite-time invariant manifolds in two dimensional velocity fields,'' ' [Chaos **11**, 427 (2001)],'' Chaos **11**, 431 (2001).
[44]E. Dresselehaus and M. Tabor, ''The kinematics of stretching and alignment of material elements in general flow fields,'' J. Fluid Mech. **236**, 415 (1991).
[45]D. G. Dritschel, P. H. Haynes, M. N. Juckes, and T. G. Shepherd, ''The stability of a two-dimensional vortex filament funder uniform strain,'' J. Fluid Mech. **236**, 647 (1991).
[46]More precisely, s and $\omega-\omega'$ are assumed to be slowly varying relative to each other.
[47]G. Lapeyre, P. Klein, and B. L. Hua, ''Does the tracer gradient vector align with the strain eigenvectors in 2-D turbulence?'' Phys. Fluids **11**, 3729 (1999).
[48]P. Klein, B. L. Hua, and G. Lapeyre, ''Alignment of tracer gradient vectors in two-dimensional turbulence,'' Physica D **146**, 246 (2000).
[49]G. Lapeyre, B. L. Hua, and P. Klein, ''Dynamics of the orientation of active and passive scalars in two-dimensional turbulence,'' Phys. Fluids **13**, 251 (2001).
[50]The averaged equation used by Pierrehumbert and Yang (Ref. 19) will only imply instability if $a(t)$ is exactly periodic and hence classic results from the theory of averaging apply.
[51]H. Chaté, E. Villermaux, and J. M. Chomaz, *Mixing—Chaos and Turbulence* (Kluwer Academic/Plenum, New York, 1999).
[52]Note that the integrals on the right-hand side of (A3) are not equal to the instantaneous net flux into B along Z^+ and Z^-, because these boundaries of B move in time.
[53]Note that when computed from (3), the lengths of $\boldsymbol{\xi}^{\pm}$ are not frame independent.
[54]A set $A\subset B$ is relatively closed in B if for any Cauchy sequence $\{a_n\}_{n=1}^{\infty}\subset A$ with $\lim_{n\to\infty}a_n=b\in B$ we have $b\in A$.
[55]For a linear system with a continuous coefficient matrix $\mathbf{A}(t)$, the solutions converging to the origin always form a manifold. This follows by noting that for any fixed time, points on such solutions form a subspace, and hence the solutions themselves form a smooth vector bundle by the smoothness of the solution operator in time and space.
[56]The existence of these manifolds was established under certain conditions. However, all those conditions are trivially satisfied in our current setting since the key parameter β appearing in the conditions vanishes.